E02-013 (GEN) Data Analysis and Archival Publication Status

Andrew Puckett

University of Connecticut

Hall A Winter Collaboration Meeting, 2019

Acknowledgements

- This talk is based on the doctoral dissertation research of Freddy Obrecht, who successfully defended his thesis on 1/4/2019
- Special thanks to Seamus Riordan (ANL) and Bogdan Wojtsekhowski (JLab) for enormous contributions to the success of this project
- Support from US Department Of Energy, Office of Science, Office of Nuclear Physics, Award ID DE-SC0014230 (Early Career research program)

Elastic *eN* scattering and form factors: formalism

$$\mathcal{M} = \frac{4\pi\alpha}{q^2}\bar{u}(k')\gamma^\mu u(k) g_{\mu\nu}\bar{u}(p')\left[F_1(q^2)\gamma^\nu + F_2(q^2)\frac{i\sigma^{\nu\alpha}q_\alpha}{2M}\right]u(p)$$

Invariant amplitude for elastic eN scattering in the one-photon-exchange approximation

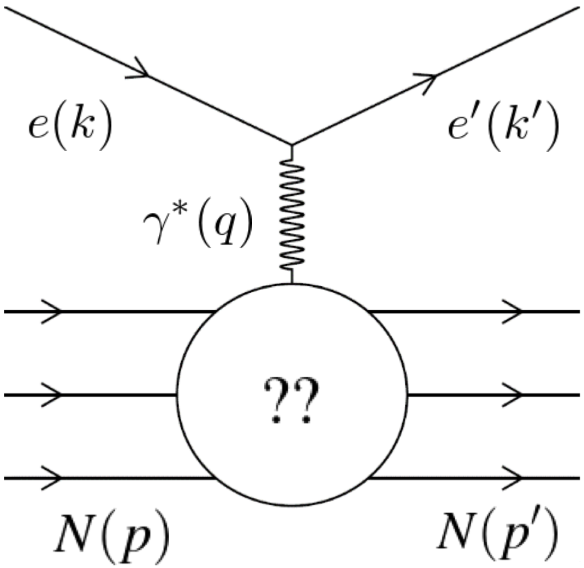

- The most general possible form of the virtual photon-nucleon vertex consistent with Lorentz invariance, parity conservation and gauge invariance is described by two form factors F_1 (Dirac) and F_2 (Pauli):
  - F_1 describes the helicity-conserving amplitude (charge and Dirac magnetic moment)
  - F_2 describes the helicity-flip amplitude (anomalous magnetic moment contribution)

$$G_E \equiv F_1 - \tau F_2$$
$$G_M \equiv F_1 + F_2$$
$$\tau \equiv \frac{Q^2}{4M^2}$$

Sachs Form Factors G_E (electric) and G_M (magnetic), are experimentally convenient linearly independent combinations of F_1, F_2

$$\frac{d\sigma}{d\Omega_e} = \frac{\alpha^2}{Q^2}\left(\frac{E'_e}{E_e}\right)^2 \cot^2\left(\frac{\theta_e}{2}\right)\left[\frac{G_E^2 + \frac{\tau}{\varepsilon}G_M^2}{1+\tau}\right]$$

$$\varepsilon^{-1} \equiv 1 + 2(1+\tau)\tan^2\left(\frac{\theta_e}{2}\right)$$

$$\sigma_R \equiv \frac{\varepsilon(1+\tau)\frac{d\sigma}{d\Omega_e}}{\left(\frac{d\sigma}{d\Omega_e}\right)_{Mott}} = \varepsilon G_E^2 + \tau G_M^2$$

Differential cross section in the nucleon rest frame:
Rosenbluth formula

Rosenbluth Separation Method: Measure cross section at fixed Q^2 as a function of ε to obtain G_E^2 (slope) and G_M^2 (intercept).

Nucleon FFs—Existing Data (ca. 2012)

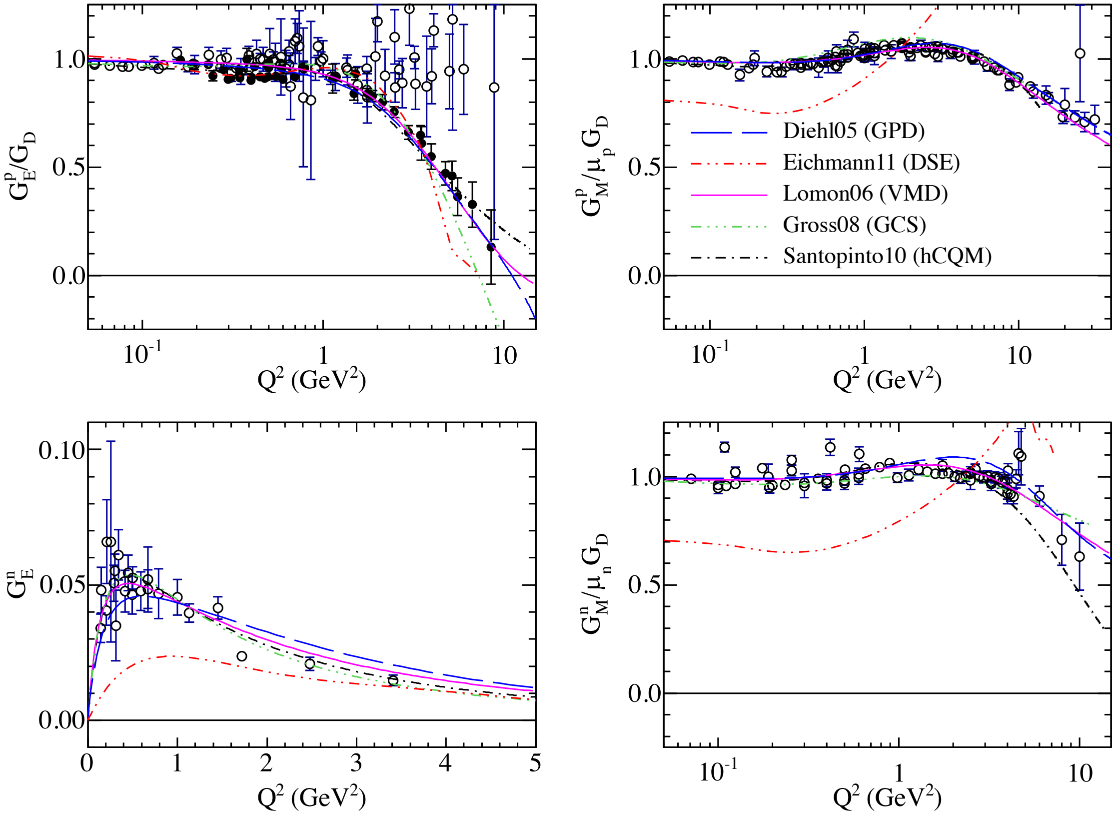

World data for G_{Ep}, G_{Mp}, G_{En}, G_{Mn} compared to selected theoretical model predictions from **Puckett *et al.*, Phys. Rev. C, 85, 045203 (2012)**

$$G_D = \left(1 + \frac{Q^2}{\Lambda^2}\right)^{-2}, \Lambda^2 = 0.71 \text{ GeV}^2$$

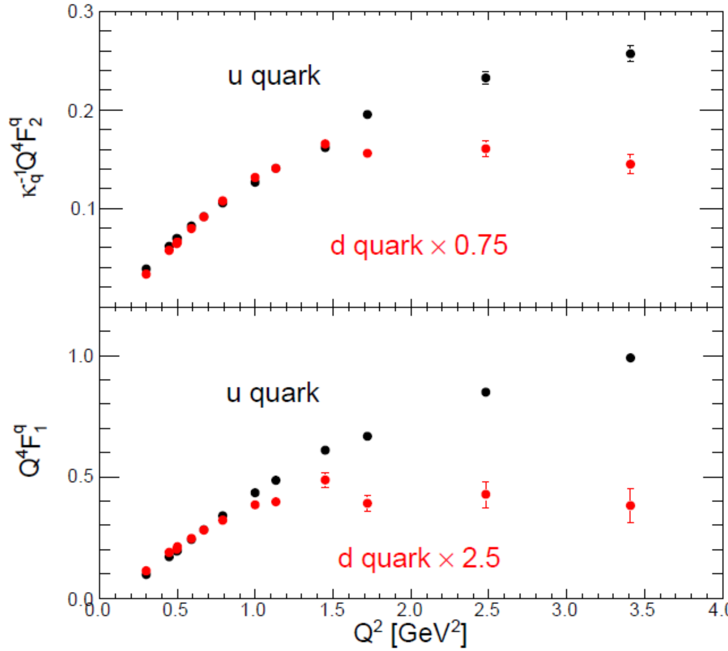

- Flavor decomposition of nucleon FFs: **Cates *et al.*, Phys. Rev. Lett., 106, 252003 (2011)**
- Different behavior of u and d quark contributions to FFs can be interpreted as a probe/signature of diquark correlations

Polarized Beam-Polarized Target Asymmetry

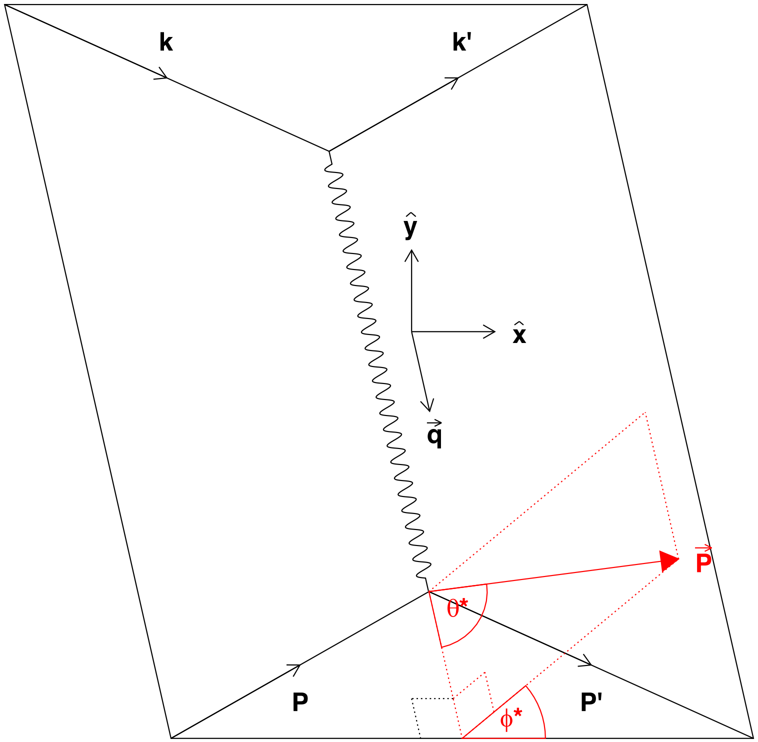

- The beam helicity asymmetry in elastic *eN* scattering from a polarized target is related to the transferred polarization by time reversal symmetry.
- The asymmetry A_t for target polarization perpendicular to the momentum transfer but parallel to the scattering plane ($\theta^* = 90°, \phi^* = 0$) equals the transverse component P_t of the transferred polarization.
- The asymmetry A_ℓ for target polarization along the momentum transfer direction ($\theta^* = 0$) is equal in magnitude but opposite in sign to the longitudinal transferred polarization P_ℓ.
- The sign change between A_ℓ and P_ℓ is due to the proton spin flip required for the absorption of the transversely polarized virtual photon

$$\vec{\mathbf{P}} \equiv \text{Target polarization}$$

$$\begin{aligned}
A_{eN} &= -\frac{P_{beam}P_{target}}{1+\frac{\epsilon}{\tau}r^2}\left[\left(\sqrt{\frac{2\epsilon(1-\epsilon)}{\tau}}\sin\theta^*\cos\phi^*\right)r + \sqrt{1-\epsilon^2}\cos\theta^*\right] \\
&\equiv P_{target}\left[A_t\sin\theta^*\cos\phi^* + A_\ell\cos\theta^*\right] \\
A_t &= P_t \\
A_\ell &= -P_\ell \\
A_n &= P_n = 0
\end{aligned}$$

Neutron form factors—G_{Mn} existing data

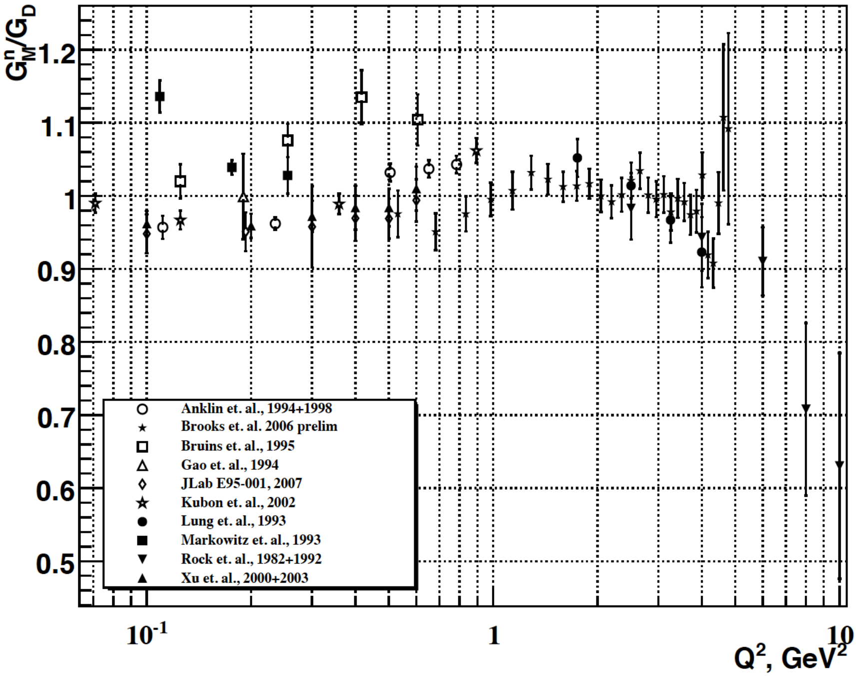

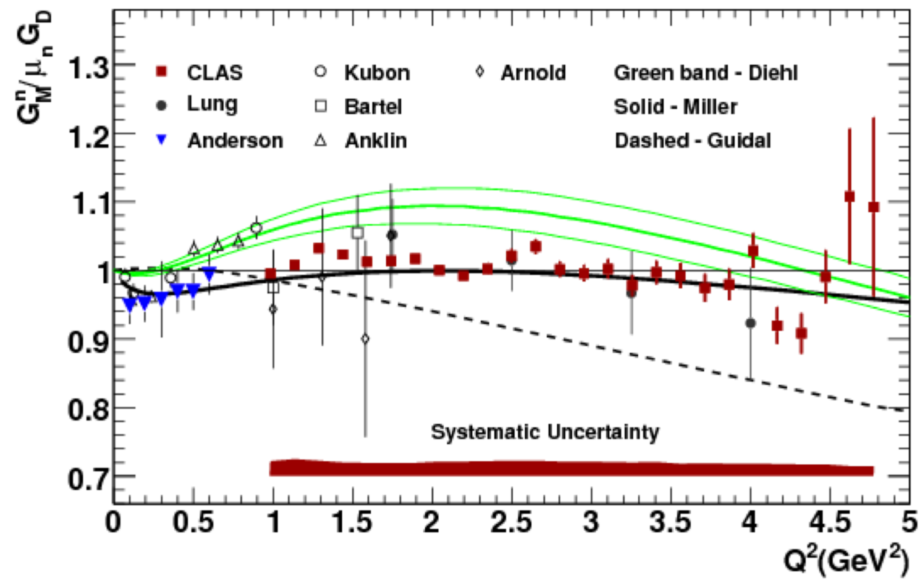

Lachniet *et al.*, CLAS Collaboration, Phys.Rev.Lett. 102 (2009) 192001

- Three main methods have been used to measure G_{Mn}:
  - "Ratio" method: measure cross section ratio of d(e,e'n)p/d(e,e'p)n in quasi-elastic kinematics
  - Absolute d(e,e'n)p quasi-elastic cross section measurement
  - Beam-target double-spin asymmetry* in inclusive quasi-elastic ^{3}He(e,e')

- **Note: double-spin asymmetry method for G_{Mn} would not work for a free neutron target, as the free nucleon asymmetry depends only on the ratio G_E/G_M, and not G_E or G_M independently.*
- Widest combined Q^2 coverage and precision from recent CLAS 6 GeV data from $1 < Q^2 < 5$ GeV^2—consistent with "standard" dipole
- Consistency issues in low-Q^2 data

Neutron form factors—G_{En} existing data

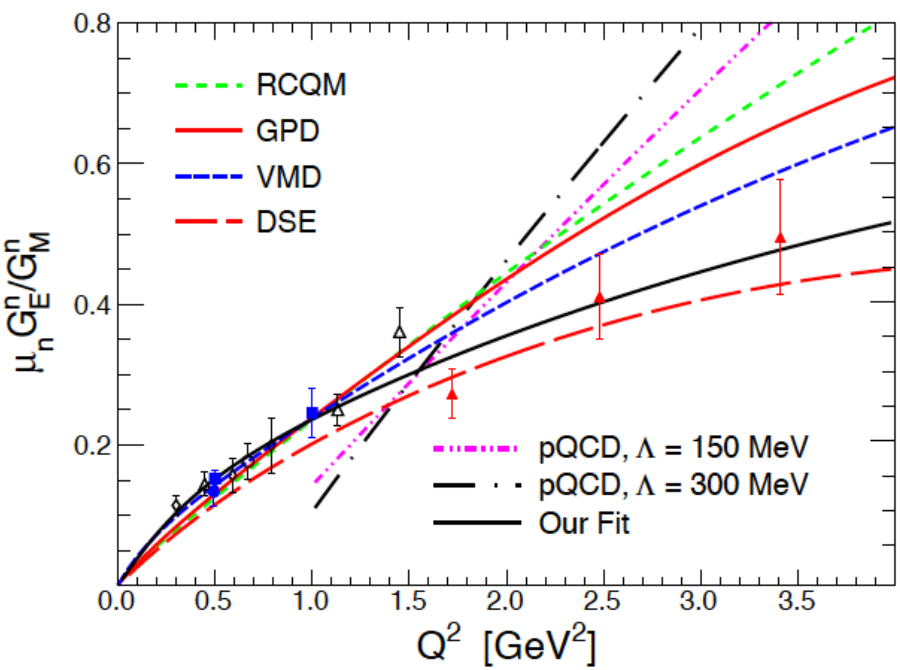

Riordan *et al.*, Phys. Rev. Lett. 105, 262302 (2010)

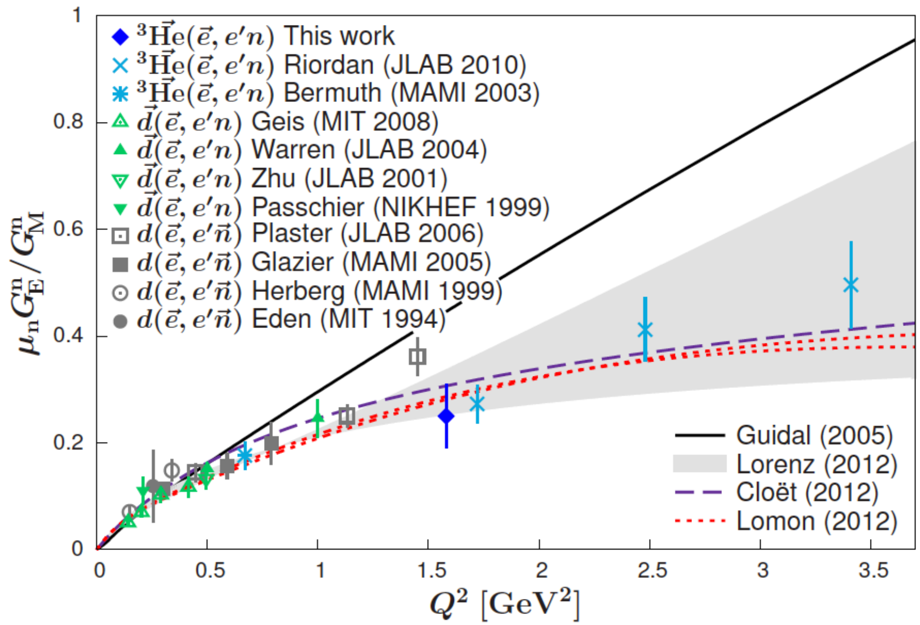

Schlimme *et al.*, Phys.Rev.Lett. 111 (2013), 132504

- G_{En} is the least well-known and most difficult to measure of the nucleon EMFFs:
  - Goes to zero at low Q^2 and cross-section contribution is small at large Q^2
- Existing knowledge (believed to be reliable) is mostly based on polarization observables:
  - Beam-target double-spin asymmetry in semi-exclusive quasi-elastic ^{3}**He**(**e**,e'n)pp
  - Beam-target double-spin asymmetry in semi-exclusive quasi-elastic ^{2}**H**(**e**,e'n)p
  - Neutron recoil polarimetery: d(**e**,e'**n**)p

Experiment E02-013 Layout (in GEANT4)

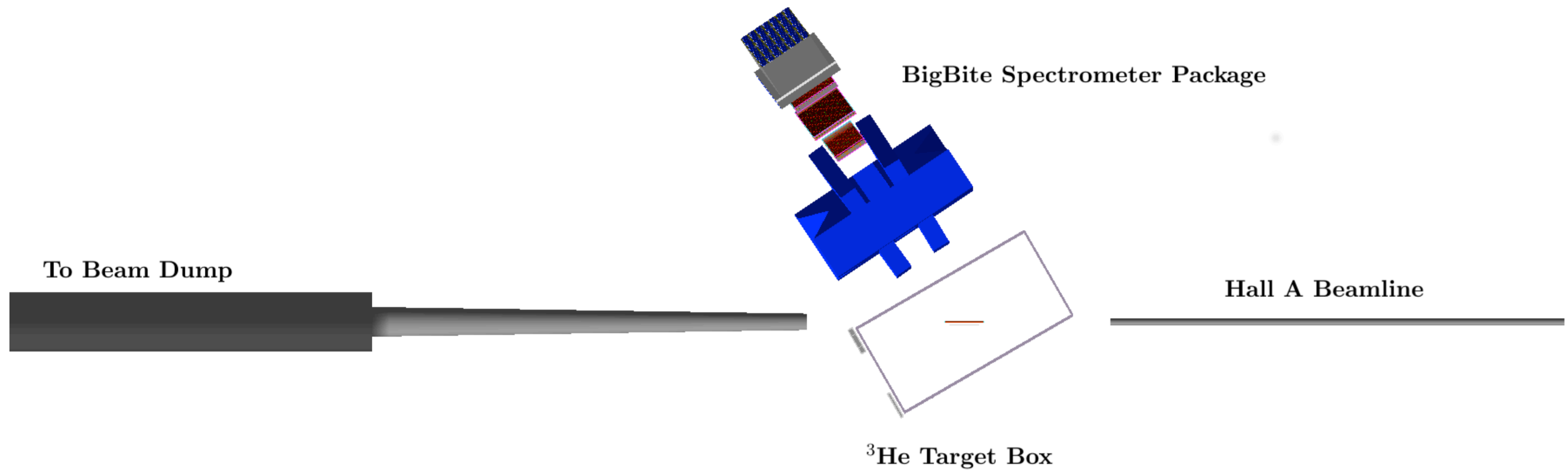

Neutron Detector

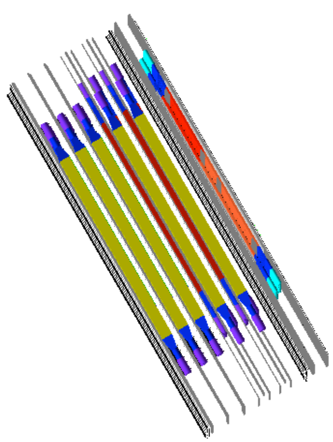

Q^2 [GeV^2]	Days	E_b [GeV]	θ_{BB} [deg]	θ_{NA} [deg]
1.16	8	1.519	-56.3	35.74
1.72	9	2.079	-51.6	35.74
2.48	19	2.640	-51.6	30.25
3.41	33	3.291	-51.6	25.63

E02-013 Kinematics: lowest Q^2 not included in PRL 2010 publication

E02-013 Analysis and Motivation

- Lowest Q^2 data were collected at the beginning of the experiment—commissioning phase of entirely new detectors/target/etc.
- Detector response/performance was initially poorly understood
- Detector calibrations were not in good shape; BigBite calorimeter and BigHAND poorly gain-matched, trigger efficiency highly nonuniform, event reconstruction poor.
- Freddy's calibrations of detectors and recooking of the low-Q^2 data ***more than doubled*** the statistics of quasi-elastic neutral coincidence events passing the cuts relative to a preliminary analysis done "over a weekend" in 2011.
- All four Q^2 points were reanalyzed with the new and improved machinery developed for the unpublished point-–no significant changes relative to original PRL publication in higher-Q^2 points

Polarized ^{3}He Target

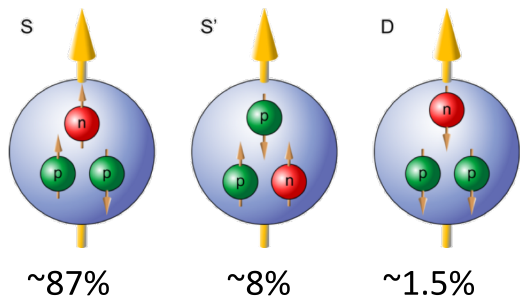

- Reminder—Polarized ^{3}He as effective polarized neutron target:
- Ground state wavefunction dominated by S-state, with unpaired neutron carrying the nuclear spin

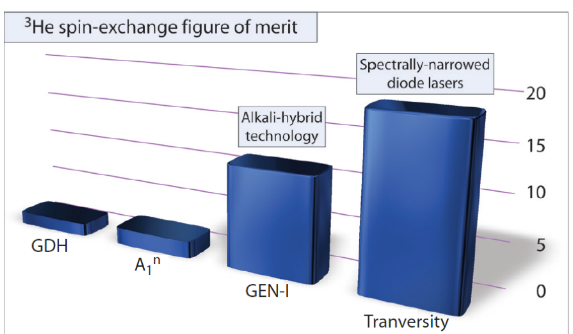

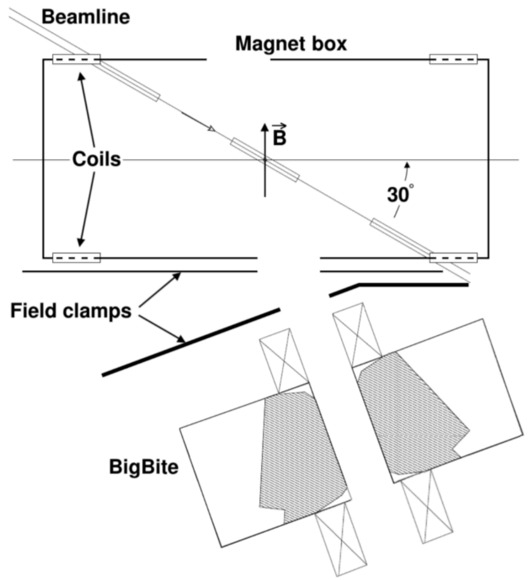

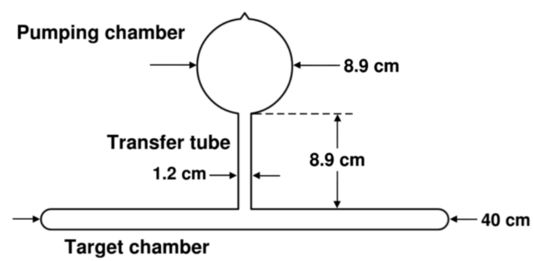

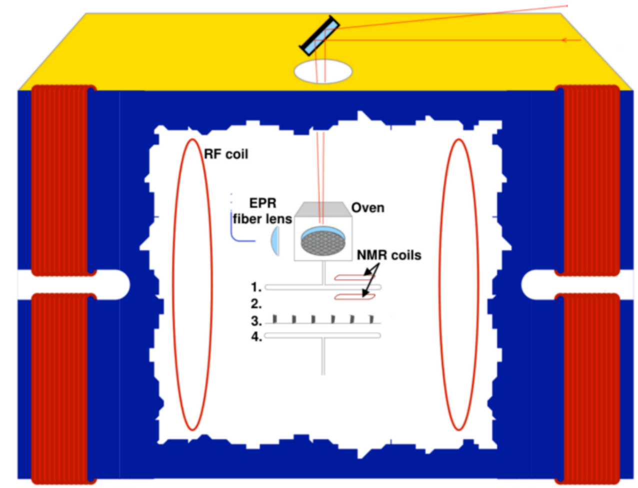

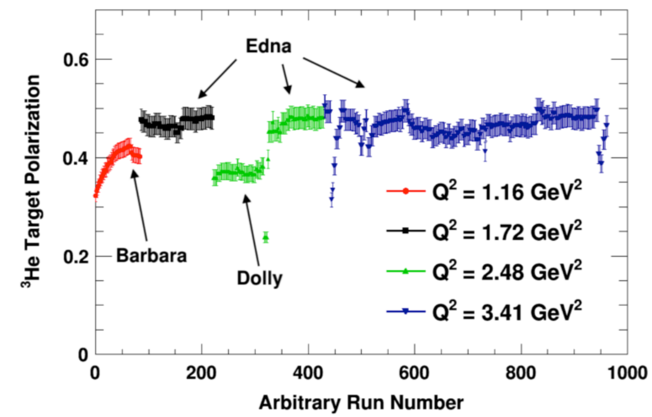

- GEN (2006) was the first electron-polarized ^{3}He scattering experiment to utilize the alkali-hybrid spin-exchange optical pumping technique to increase figure-of-merit.

Electron and Nucleon Detection

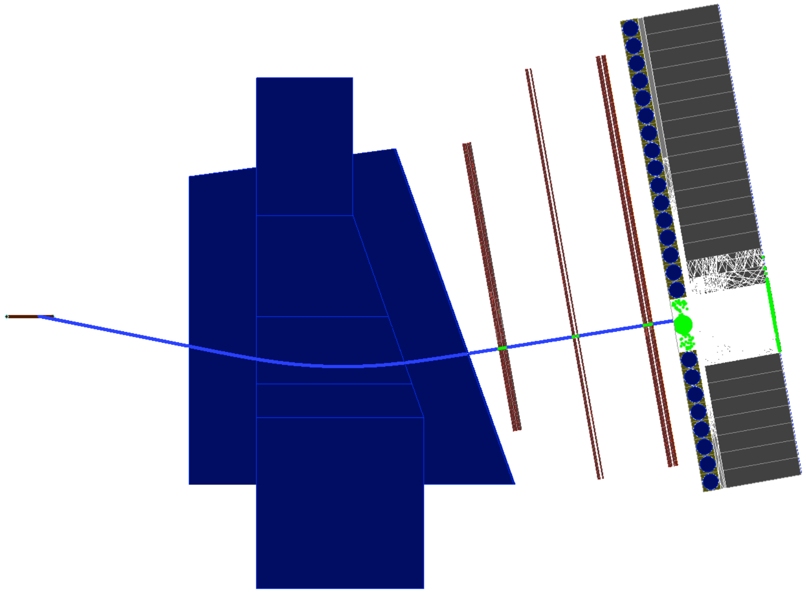

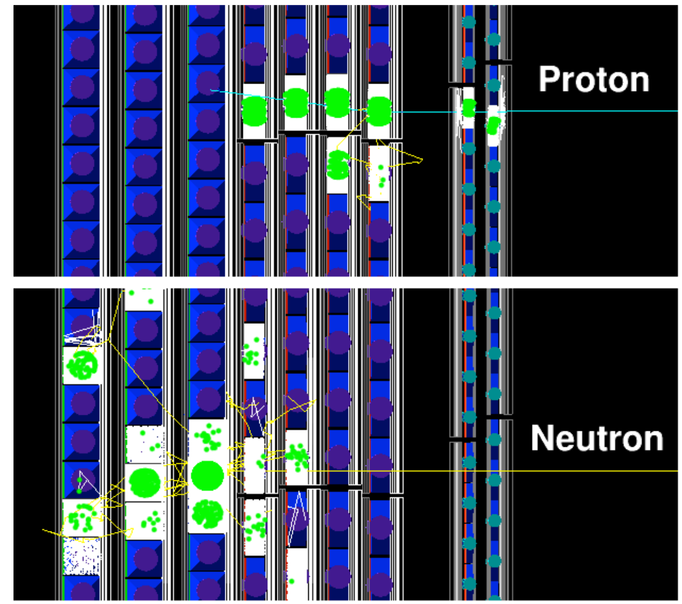

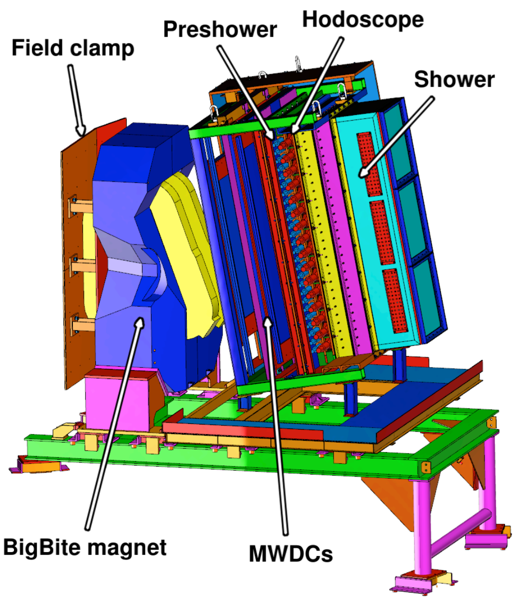

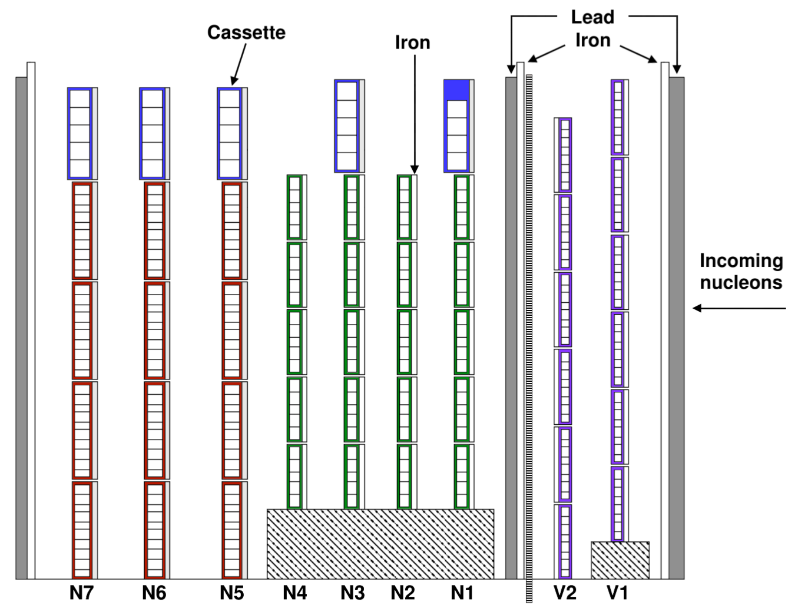

Quasi-elastic Event Selection: ^{3}He data, $Q^2 = 1.16$ GeV^2

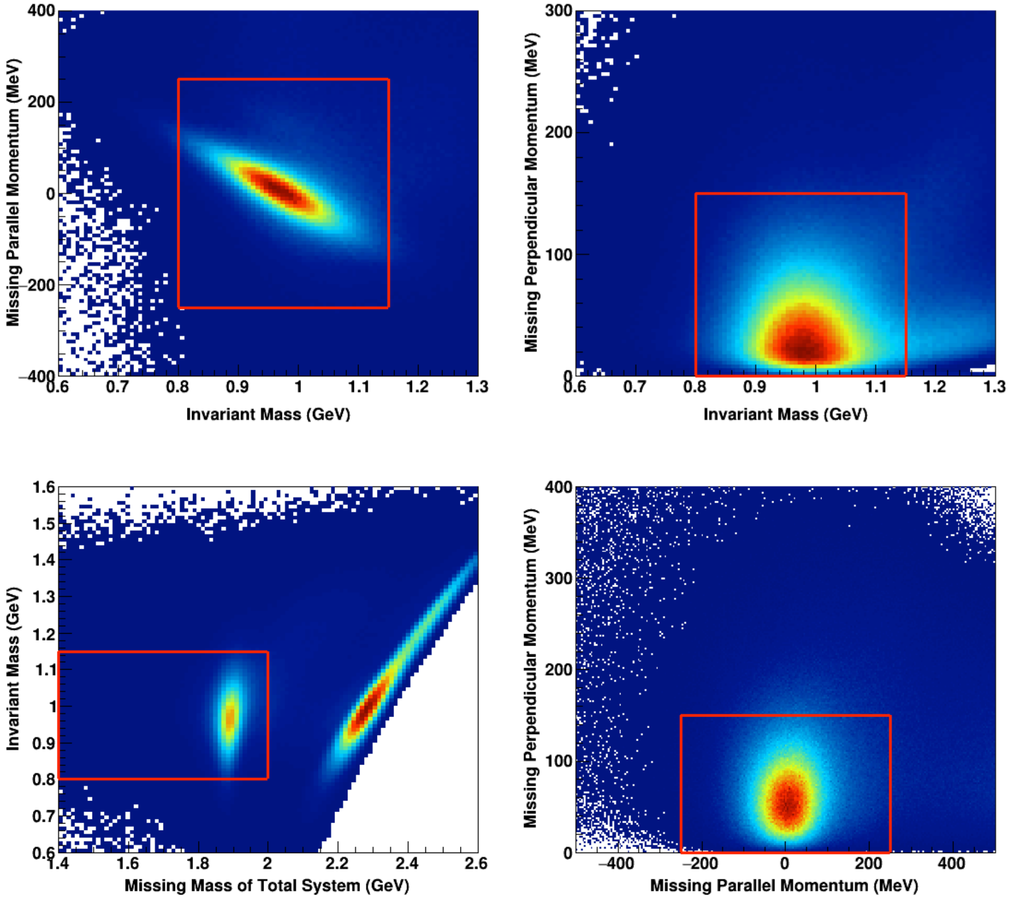

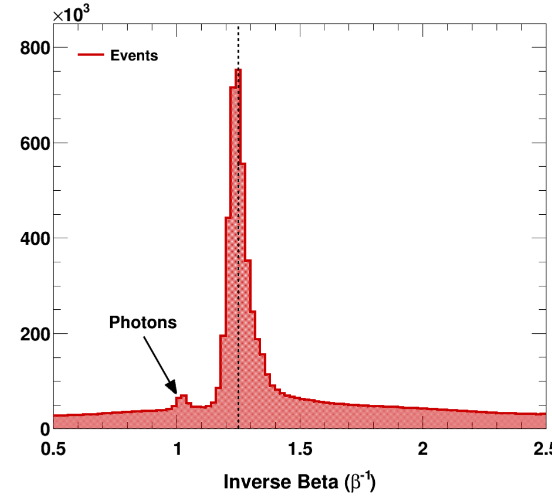

- Nucleon identification and momentum reconstruction via time-of-flight

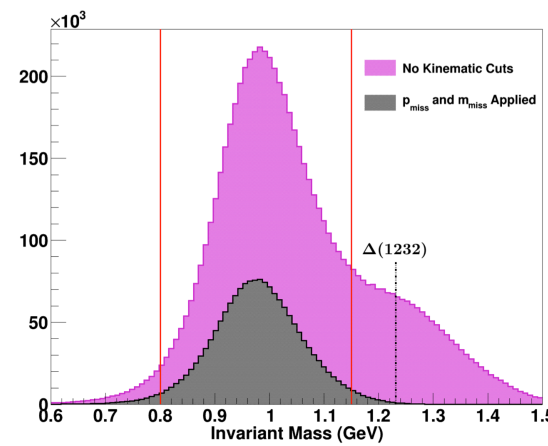

$Q^2 = 1.16\ \mathrm{GeV}^2$

- Three main cuts to select the coincidence quasi-elastic channel: Invariant mass W, missing parallel and perpendicular momentum, and "missing mass"

- W distribution before and after cuts

Quasi-elastic coincidence event selection: All kinematics

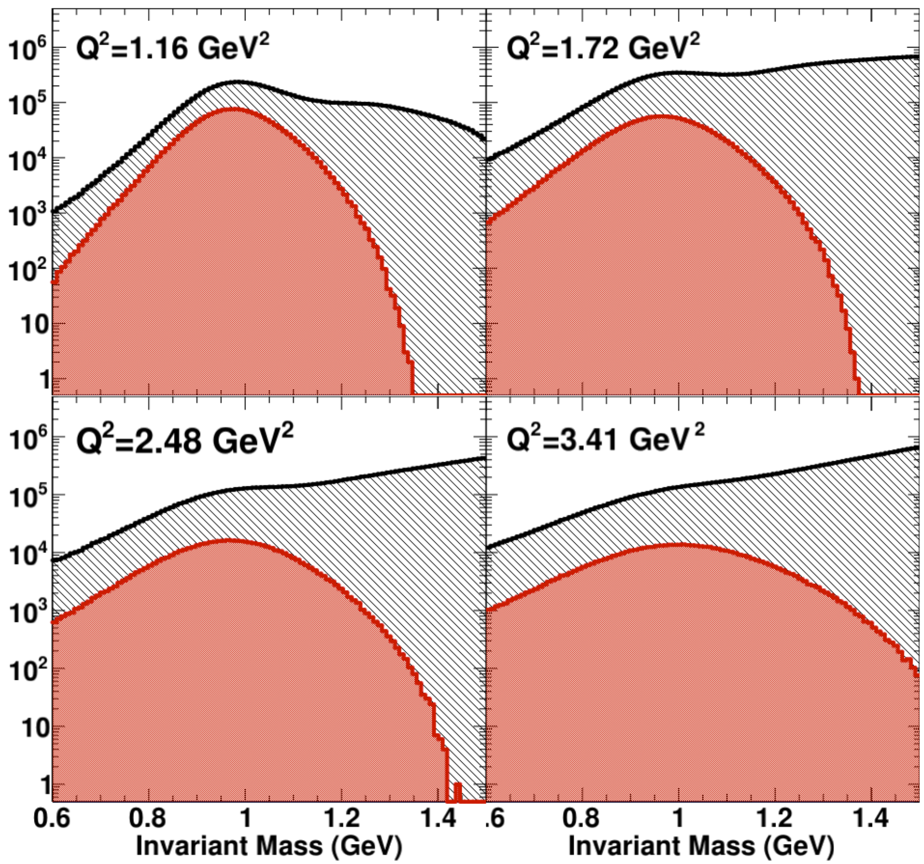

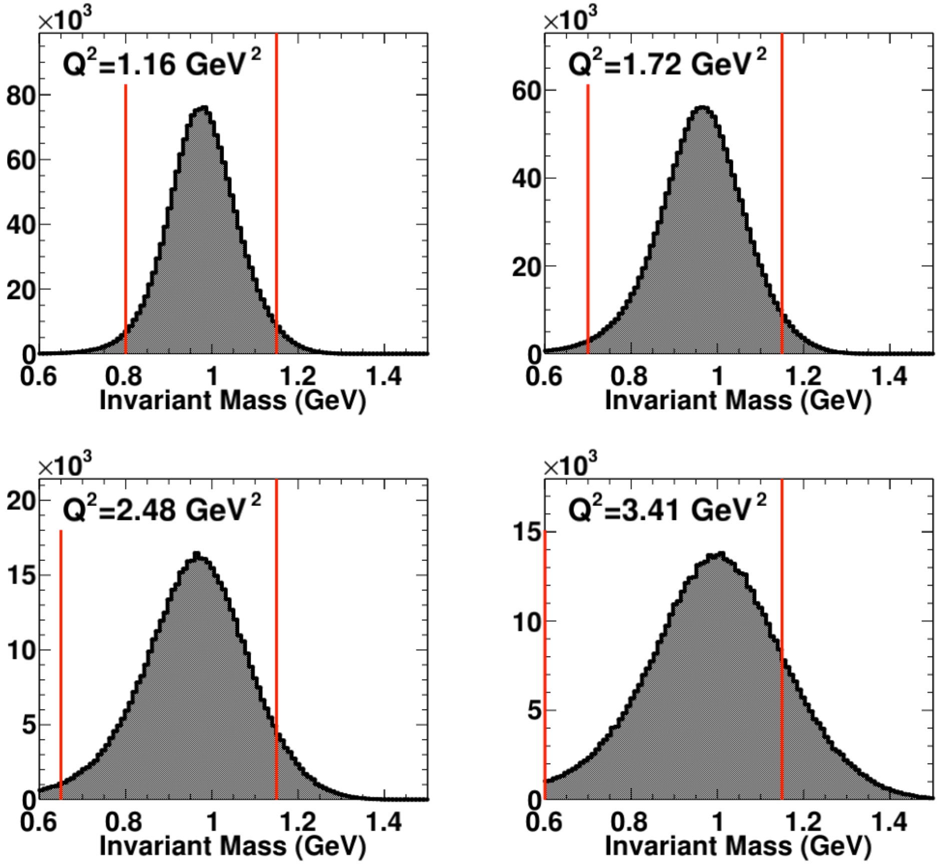

- Width of quasi-elastic W distribution due to Fermi smearing increases with Q^2.
- Inelastic scattering yield relative to quasi-elastic also increases with Q^2.
- Nevertheless, two-arm coincidence and exclusivity cuts result in a very clean selection of QE events at all four Q^2

Raw Asymmetries

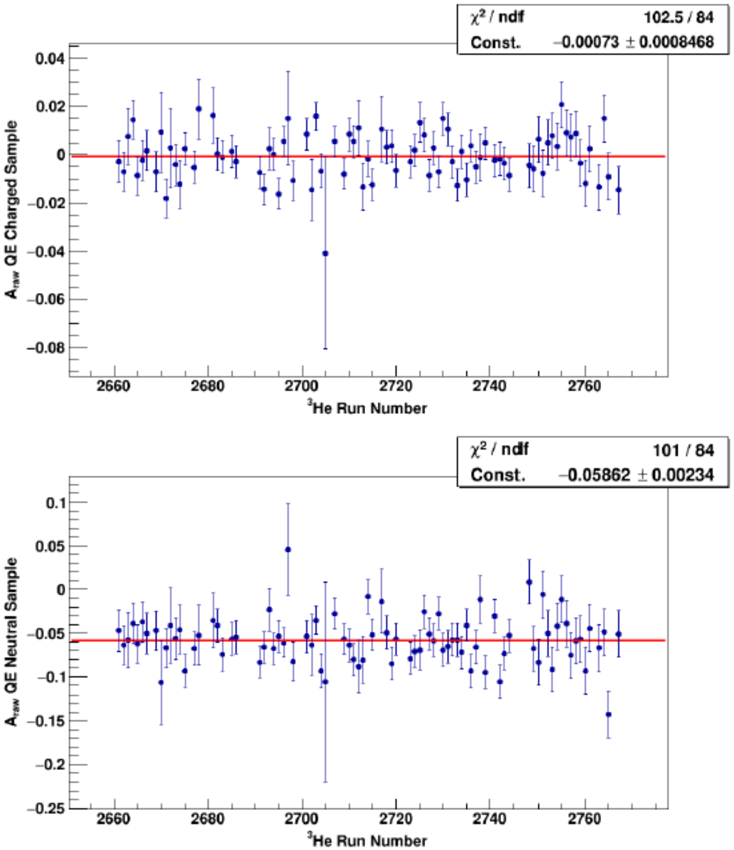

Fig. 5.62: The raw asymmetry for the QE charged (top panel) and uncharged (bottom panel) samples over the ^{3}He data set. The raw asymmetry for the charged sample is expected to be much smaller than the uncharged sample.

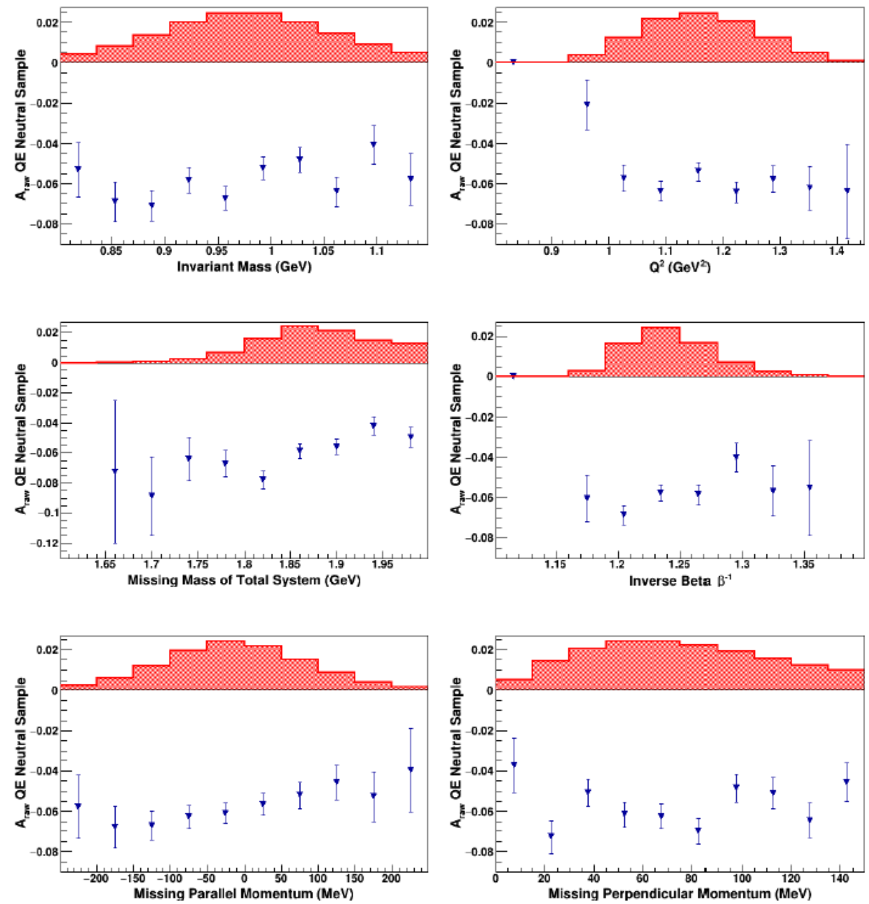

Fig. 5.63: A comparison of A_{raw} to important kinematic variables which are represented by the shaded red regions and have been scaled to fit; therefore, the y-axis is arbitrary for kinematic relations.

Raw asymmetry to "physics" asymmetry—Summary of Dilution Factors/Corrections

Parameter	Value	Description
P_{beam}	0.872 ± 0.020	Beam polarization
$P_{^3\mathrm{He}}$	0.397 ± 0.015	Target polarization
D_{bk}	0.949 ± 0.029	Accidental background
$D_{\mathrm{N_2}}$	0.954 ± 0.005	N_2 in ^{3}He cell
D_{p}	0.812 ± 0.017	Proton misidentification
D_{π}	0.997 ± 0.001	Preshower pion dilution
D_{in}	1.000 ± 0.050	Inelastic dilution
D_{FSI}	0.977 ± 0.020	Nuclear corrections
$\frac{\Delta_{\mathrm{bk}}}{\Sigma}$	-0.0003 ± 0.0005	Background asymmetry correction
$\frac{\Delta_{\mathrm{p}}}{\Sigma}$	-0.0008 ± 0.0004	Proton asymmetry correction
$\frac{\Delta_{\pi}}{\Sigma}$	-0.0002 ± 0.0001	Preshower pion asymmetry
A_{in}	0.0000 ± 0.0150	Inelastic asymmetry correction
A_{FSI}	-0.0012 ± 0.0008	Nuclear corrections
N_{qe}	1.816×10^5	Total # of quasielastic events
A_{raw}	-0.0584 ± 0.0023	Raw asymmetry
A_{phys}	$-0.2291 \pm 0.0094 \pm 0.0129$	Physical asymmetry ± stat ± sys

Table 6.11: All parameters used in the calculation of A_{phys}. Recall that the effects of nuclear polarization are embedded within the nuclear corrections.

- See backup slides for more plots/details
- Most significant dilution factors:
  - Accidental coincidence background
  - Nitrogen dilution
  - Proton misidentification
- Others include FSI, inelastic contamination, and BigBite pions. The latter two are basically negligible.

Nuclear corrections—Mainly FSI

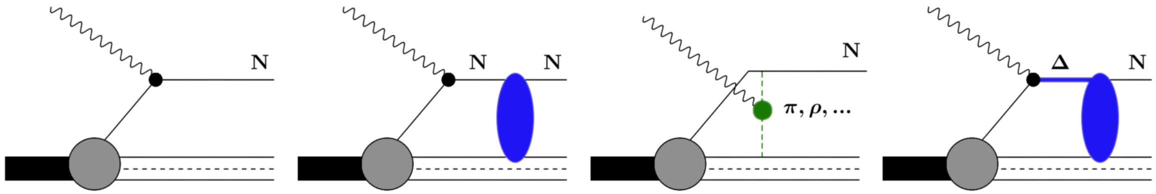

Figure A Figure B Figure C Figure D

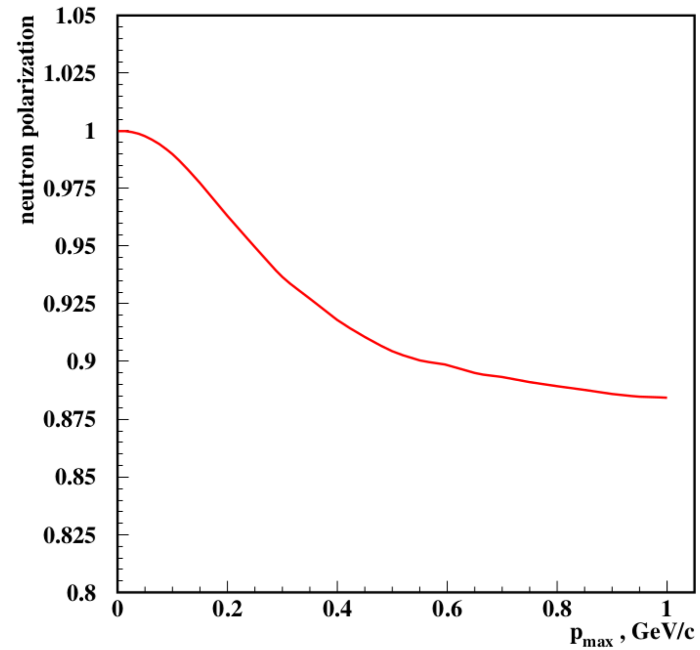

- Nuclear corrections calculated within Generalized Eikonal Approximation framework
  - Cross section/asymmetry calculation code provided by Misak Sargsian (FIU)
  - Event-by-event MC simulation folded with experimental acceptance—lots of numerical integration, computationally expensive! (Much easier to do with 2019 JLab scientific computing facilities than 2009)
- A: PWIA
- B: FSI/charge-exchange
- C: Meson Exchange Currents
- D: Isobar Configurations
- Diagrams "A" and "B" dominant in E02-013 kinematics
- Exclusivity selection increases effective neutron polarization from the canonical 86% (of P_{He}) in the inclusive case to 96% in the coincidence—quasi-elastic case.

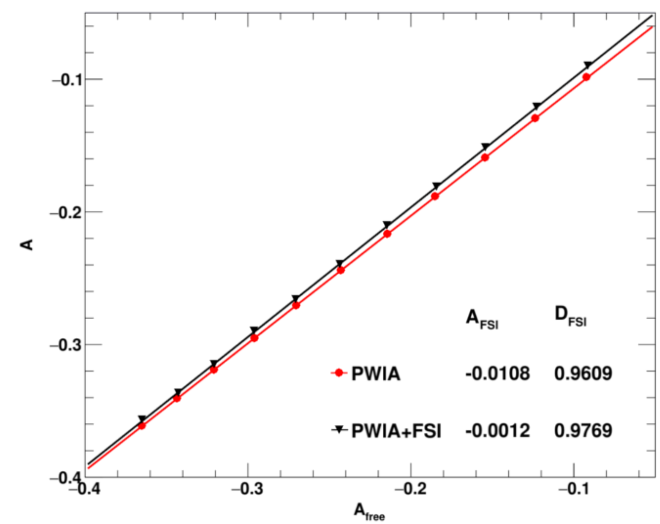

GEN Nuclear Effects Compute Farm Stats

- In calendar 2018, the GEN nuclear corrections calculations accounted for approximately 25% of Hall A batch farm usage by process-hours.
- Essentially ALL of this was the nuclear corrections; no reconstruction, no analysis
- Nuclear corrections redone for all four Q^2 points with higher MC statistics, better precision/accuracy, exploiting a decade of improvements in batch farm capacity.
- No major changes in nuclear corrections observed since 2009

Scicomp Farm Cluster Usage (org to project view)

Change time period: 01/01/2018 - 12/31/2018

Usage (org-project) | Usage (org-type) | Usage (type-org)

All halla Jobs

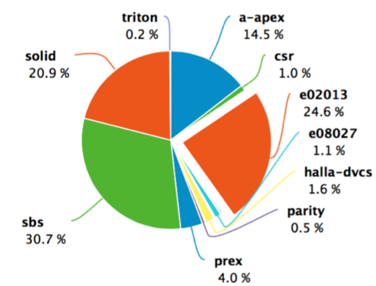

Org	Project	Job Count	Process Hour
accelerator	all	20,021	159,696
casa	all	454,659	1,274,332
cc	all	44	1,478
clas	all	1,257,701	2,681,253
clas12	all	1,179,515	16,228,700
eic	all	48,514	196,923
eshq	all	4,926	32,828
halla	all	4,111,317	4,973,007
halla	a-apex	465,251	723,079
halla	csr	156,647	51,627
halla	e02013	577,250	1,221,710
halla	e05102	2,406	14,896
halla	e07006	4,524	7,547
halla	e08027	2,043	54,173
halla	g2p	1,240	3,217
halla	gdh	395	75
halla	GMP12	50,602	11,770
halla	halla-dvcs	11,921	80,199
halla	moller12gev	20,733	6,373
halla	parity	31,612	26,353
halla	prex	112,970	197,527
halla	sbs	199,342	1,528,967
halla	solid	2,426,125	1,037,798
halla	triton	48,256	7,694
hallb	all	2,268,365	3,310,676
hallc	all	1,086,381	1,360,372
halld	all	5,125,633	41,365,347
theory	all	17,168	498,769
		15,574,244	72,083,381

Extraction of G_E^n from A_{phys}^{en}--target spin direction measurement

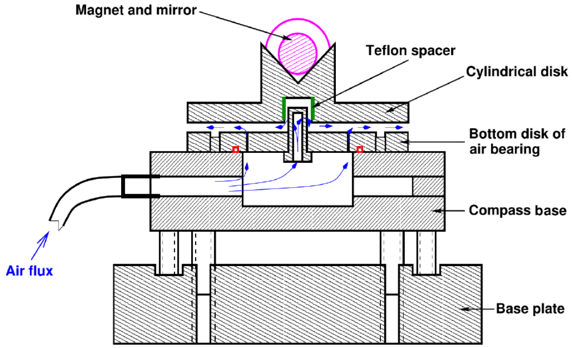

FIG. 10. (color online) The compass developed to accurately measure the direction of the magnetic holding field. The various plates and disks were constructed from aluminum, and the strong permanent magnetic and mirror were able to rotate freely on a cylindrical air bearing and piston design.

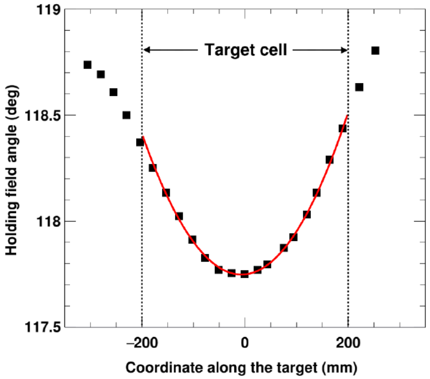

FIG. 11. The direction of the holding magnetic field along the target cell, where the angle is defined to be the counter clockwise angle between the beamline direction and the direction of the holding field.

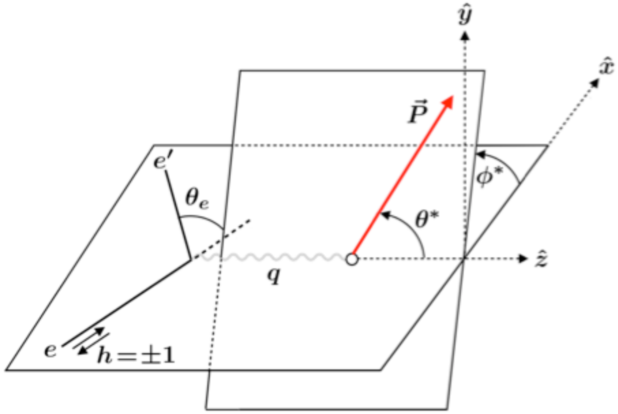

$$
\begin{aligned}
A_{eN} &= -\frac{P_{beam}P_{target}}{1+\frac{\epsilon}{\tau}r^2}\left[\left(\sqrt{\frac{2\epsilon(1-\epsilon)}{\tau}}\sin\theta^*\cos\phi^*\right)r+\sqrt{1-\epsilon^2}\cos\theta^*\right] \\
&\equiv P_{target}\left[A_t\sin\theta^*\cos\phi^*+A_\ell\cos\theta^*\right] \\
A_t &= P_t \\
A_\ell &= -P_\ell \\
A_n &= P_n = 0
\end{aligned}
$$

$$
r \equiv \frac{G_E^n}{G_M^n}
$$

Q^2 [GeV^2]	Days	E_b [GeV]	θ_{BB} [deg]	θ_{NA} [deg]
1.16	8	1.519	-56.3	35.74
1.72	9	2.079	-51.6	35.74
2.48	19	2.640	-51.6	30.25
3.41	33	3.291	-51.6	25.63

- Asymmetry is a nonlinear function of FF ratio *r*. Born approximation formula defines a quadratic equation for *r* with an analytic solution (but also sign ambiguity).
- Optimal sensitivity to *r* when target polarization is orthogonal to $\vec{q}$, parallel to scattering plane.

Results

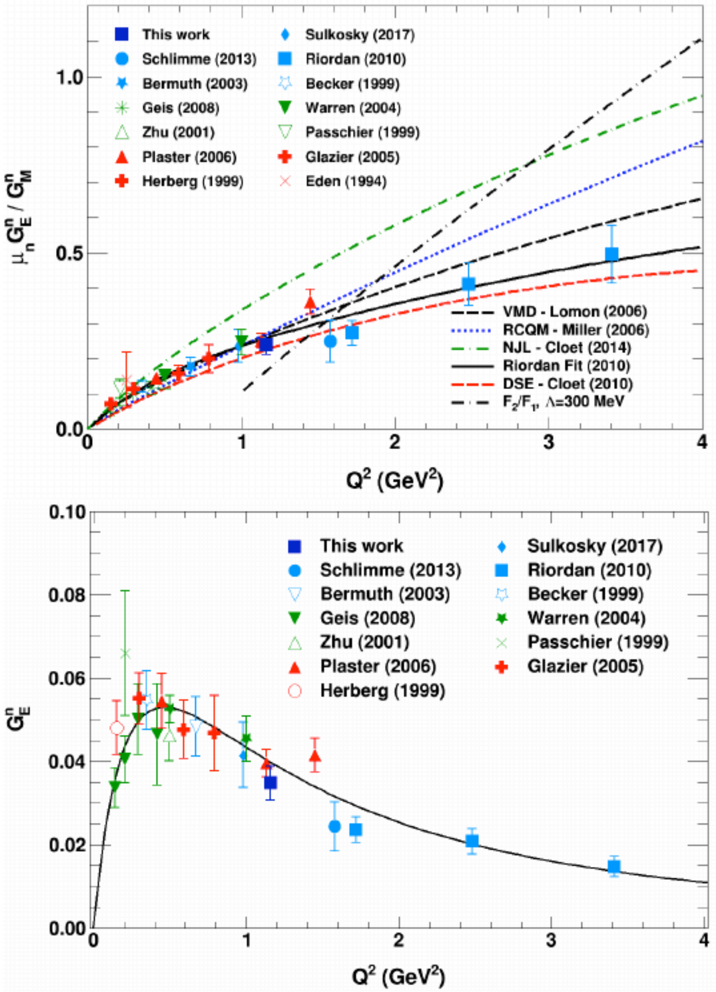

Source	δ/G_E^n	Comments
δG_E^n	0.123	Total uncertainty contribution
δ_{sys}	0.100	Systematic
δ_{stat}	0.071	Statistical
$\delta P_{^3\text{He}}$	0.067	Target polarization
δP_{beam}	0.040	Beam polarization
δD_{FSI}	0.035	Nuclear corrections
δD_{bk}	0.029	Background dilution
δD_{p}	0.028	Proton dilution
δG_M^n	0.025	Error from chosen G_M^n
δ_{other}	0.023	Remaining contributions

- Result at 1.16 GeV^2 consistent with other data in this region.
- Total uncertainty ~12% relative. Systematics dominated by target polarization. Statistical error slightly smaller than total systematics.

Summary and Conclusions

- Draft archival publication (Phys. Rev. C) in preparation, ~90% complete (very much in editing and proofreading stage)
- Analysis is complete and final, up to finalizing the target polarization systematics for the lowest Q^2 point.
- Completion of low-Q^2 analysis and archival publication of whole experiment brings closure to E02-013
- Consistency of low-Q^2 data with existing overlapping data also increases confidence in validity of high-Q^2 data (not that they were in doubt…).
- Expect archival paper submission to PRC in first half of 2019
- Thank you for your attention!

Backup Slides

Polarization Transfer in Elastic *eN* scattering

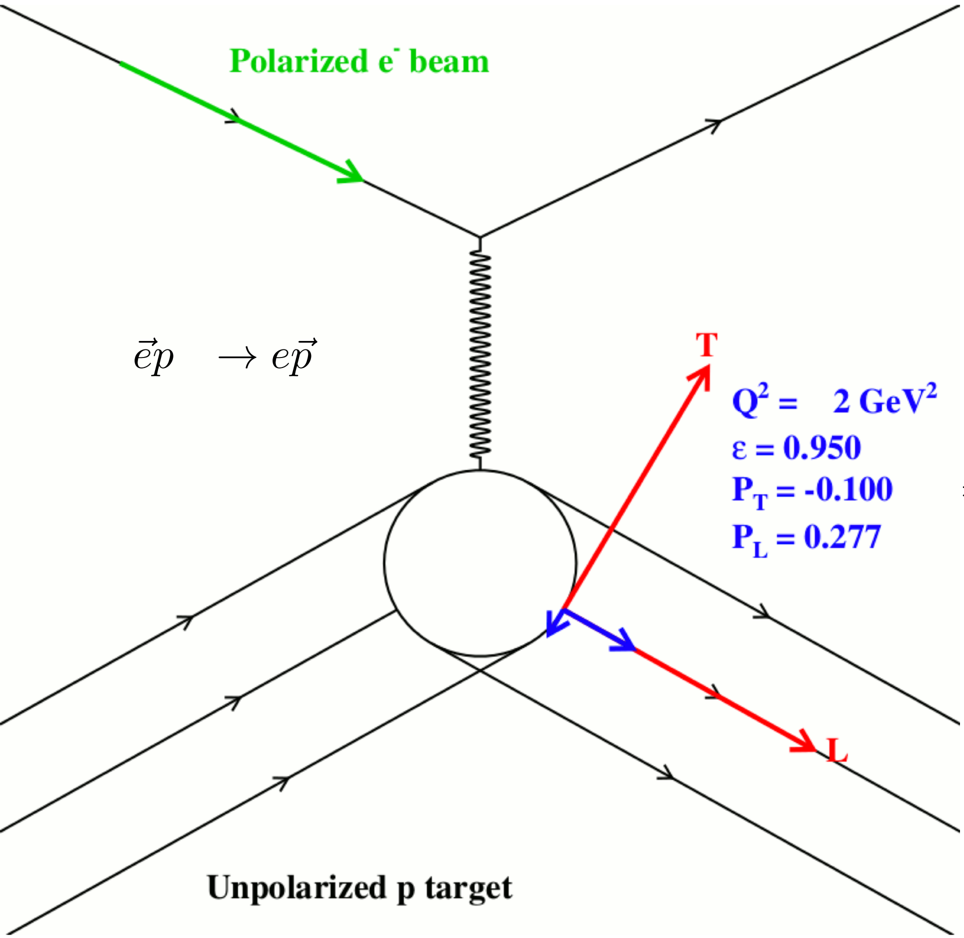

$$P_t = -P_{beam}\sqrt{\frac{2\epsilon(1-\epsilon)}{\tau}}\frac{r}{1+\frac{\epsilon}{\tau}r^2}$$

$$P_\ell = P_{beam}\frac{\sqrt{1-\epsilon^2}}{1+\frac{\epsilon}{\tau}r^2}$$

$$P_n = 0$$

$$r \equiv \frac{G_E}{G_M}$$

$$\Longrightarrow R_p \equiv \mu_p \frac{G_E^p}{G_M^p} = -\mu_p\sqrt{\frac{\tau(1+\epsilon)}{2\epsilon}}\frac{P_t}{P_\ell}$$

- Akhiezer and Rekalo (1968) + Arnold, Carlson, Gross (1981):
  - ***Derived the relations between transferred polarization components in elastic eN scattering and the ratio of electromagnetic FFs $R = \mu G_E/G_M$***
- Perdrisat + Punjabi, 1993 proposal to CEBAF PAC: A ***simultaneous*** measurement of the two recoil polarization components in a polarimeter determines the FF ratio while canceling many systematic uncertainties (beam polarization, analyzing power, FPP instrumental asymmetry)

- ***The ratio of transferred polarization components is directly proportional to G_E/G_M, and therefore much more sensitive to G_E at large Q^2 than the cross section***

Proton FFs—Rosenbluth data

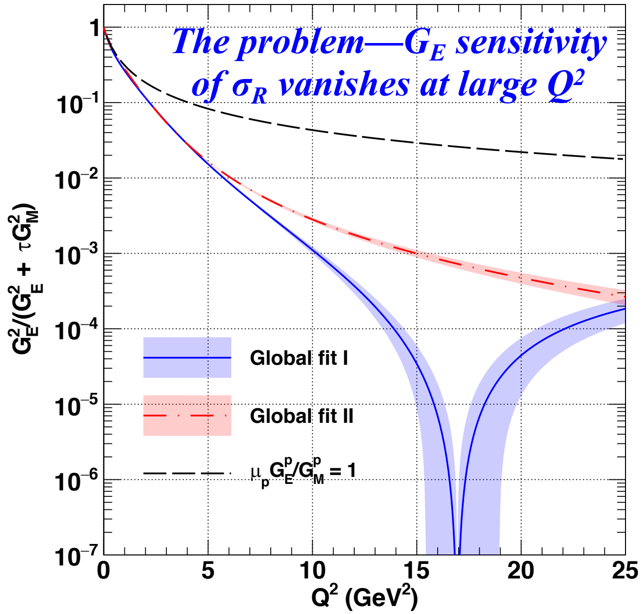

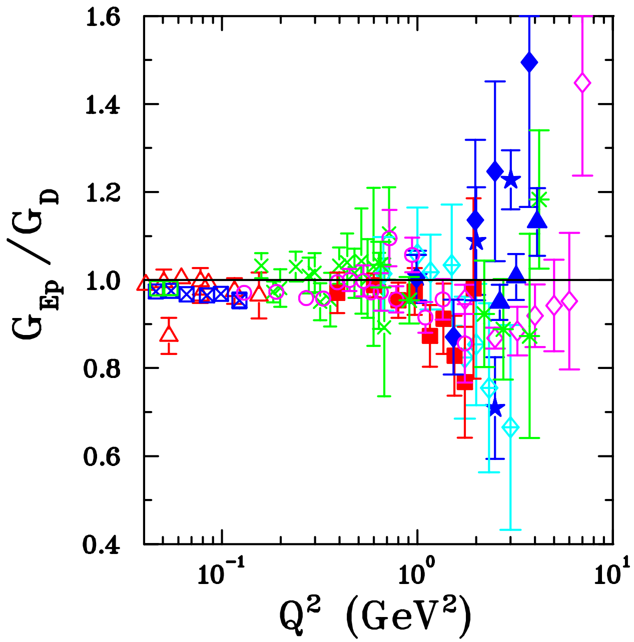

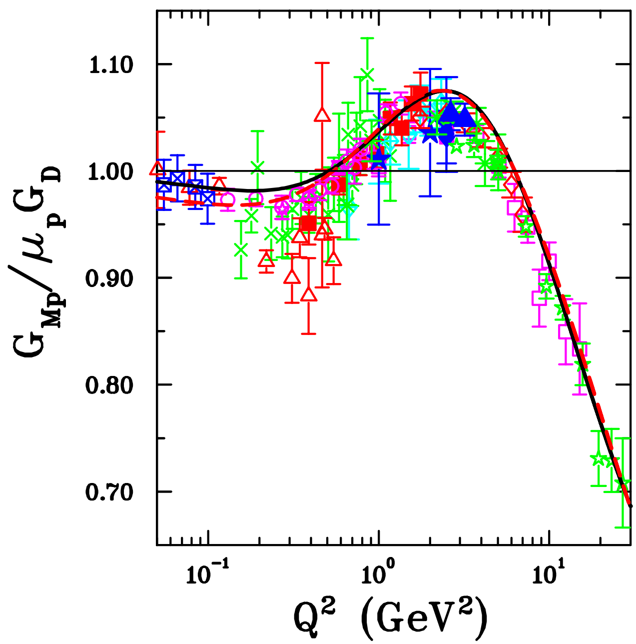

Maximum contribution of G_E^2 term to σ_R vanishes at large τ. Fits to FF data are described in [Phys. Rev. C, 96, 055203 (2017)] (more on these later)

$$\sigma_R = \epsilon G_E^2 + \tau G_M^2$$

G_E^p and G_M^p Rosenbluth Data: $G_E^p \approx \frac{G_M^p}{\mu_p} \approx G_D$

$$G_D \equiv \left(1 + \frac{Q^2}{\Lambda^2}\right)^{-2}$$
$$\Lambda^2 = 0.71 \text{ GeV}^2$$

- Elastic *ep* cross sections have been measured for $0.003 \leq Q^2 \leq 31.2$ GeV^2.
- Rosenbluth data for G_E^p and G_M^p are qualitatively described by the "dipole" form factor, which is the Fourier transform of a spherically symmetric, exponentially decreasing radial charge/magnetization density.

Proton FFs—Polarization Data

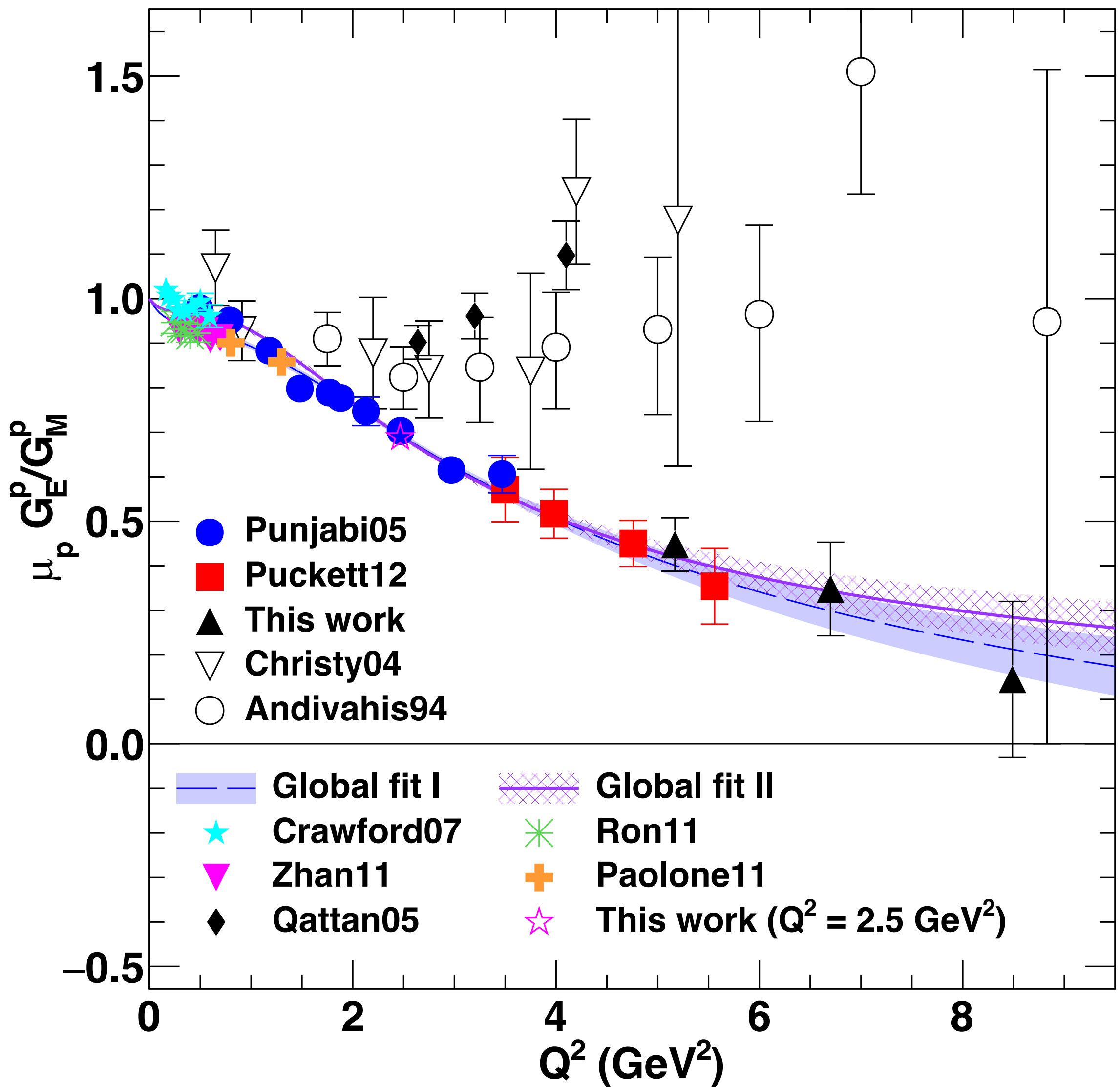

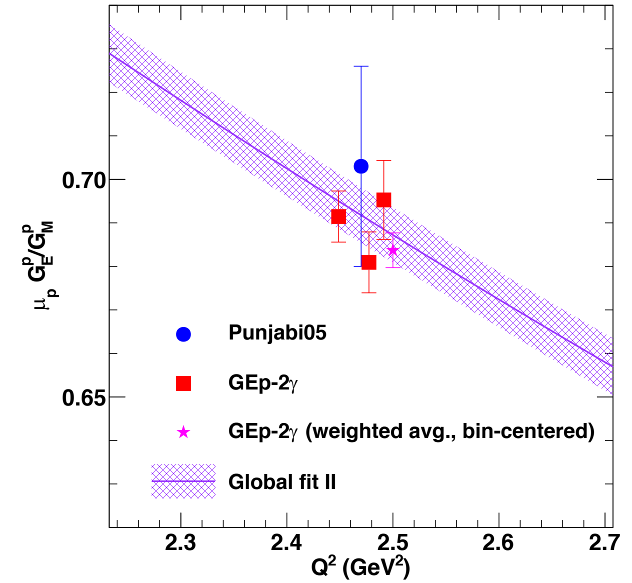

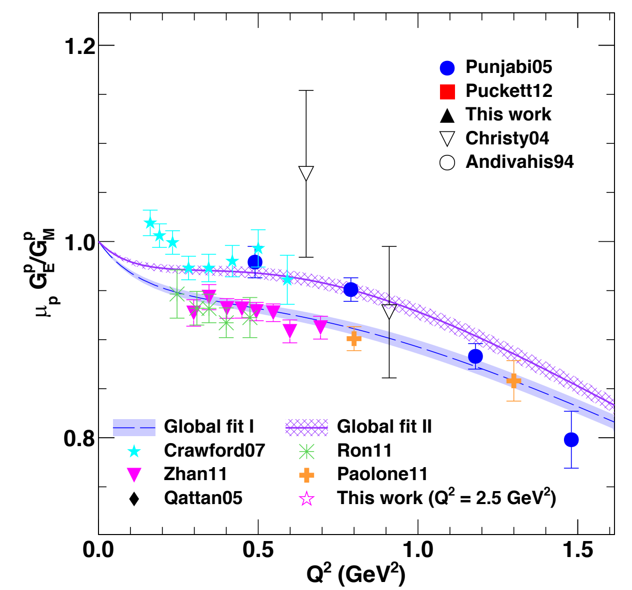

GEp-III/GEp-2γ final results (Puckett *et al.*, Phys. Rev. C 95, 055203 (2017))

Kin. 1 Calibrations and reconstruction improvements—BigBite preshower and shower

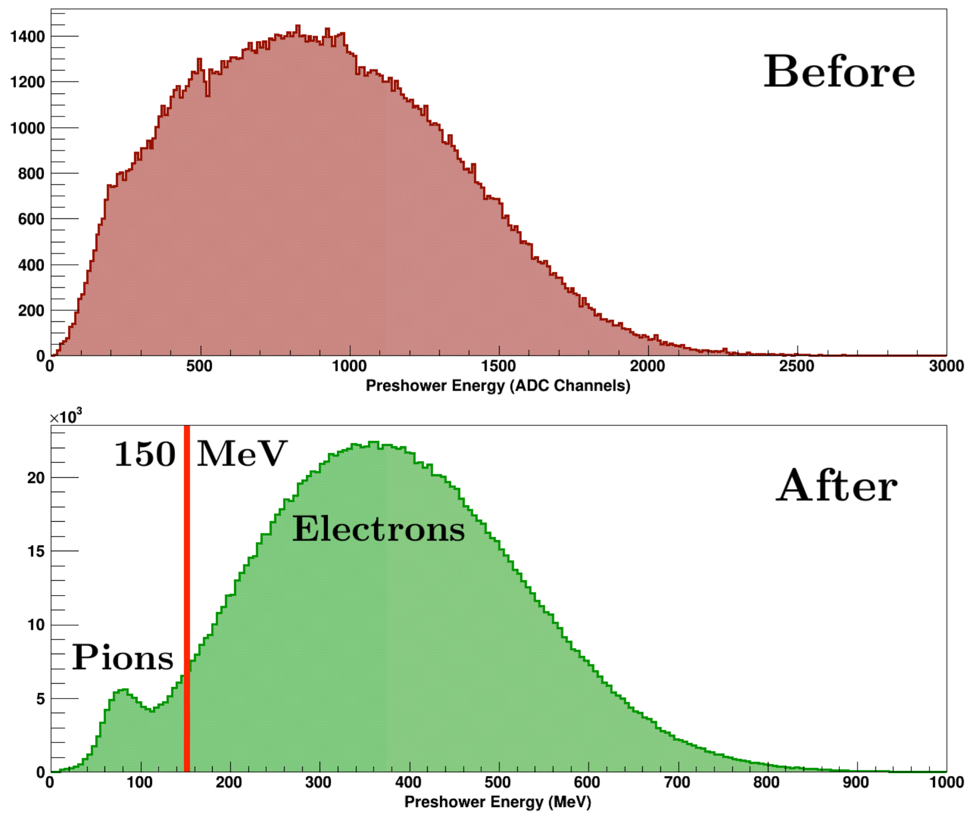

Preshower Energy Calibration

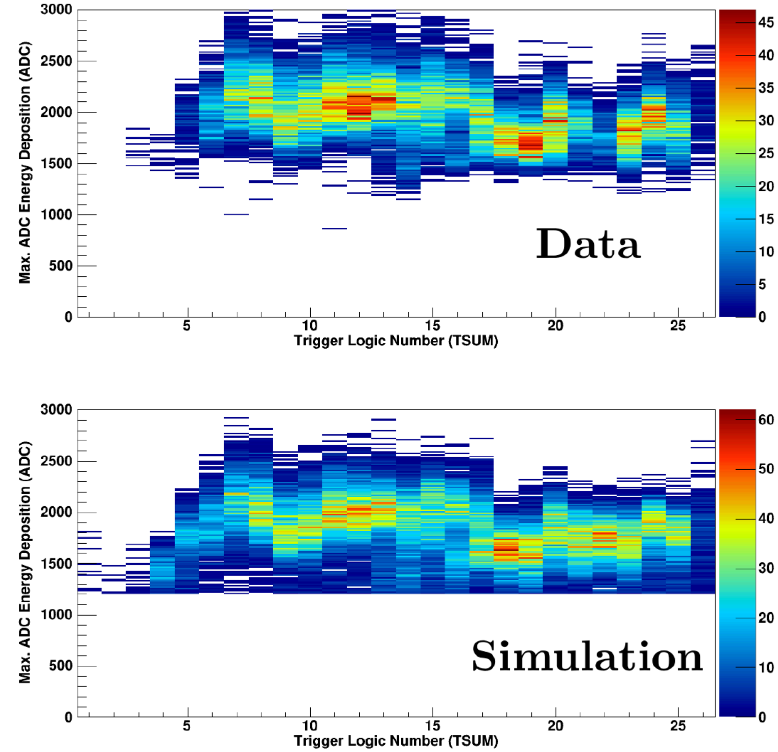

- BigBite Trigger Logic Sums—poor initial gain matching and calibration leads to non-uniform trigger efficiency/"gaps"
- After calibration, this is reproducible in simulation—important for dilution analysis

Kin. 1 Calibrations—Summary

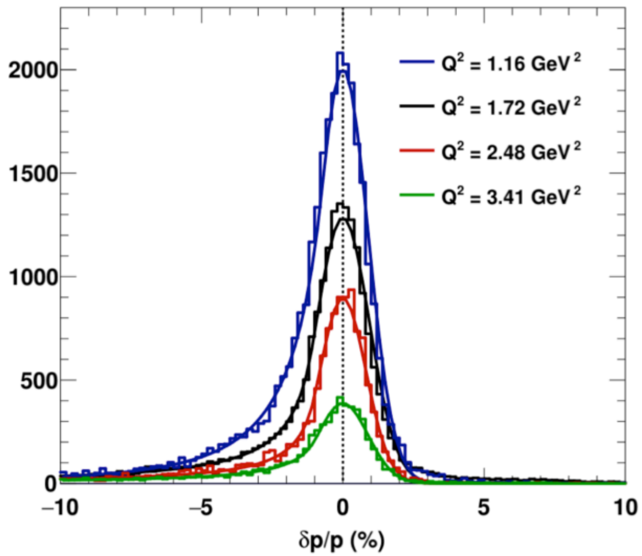

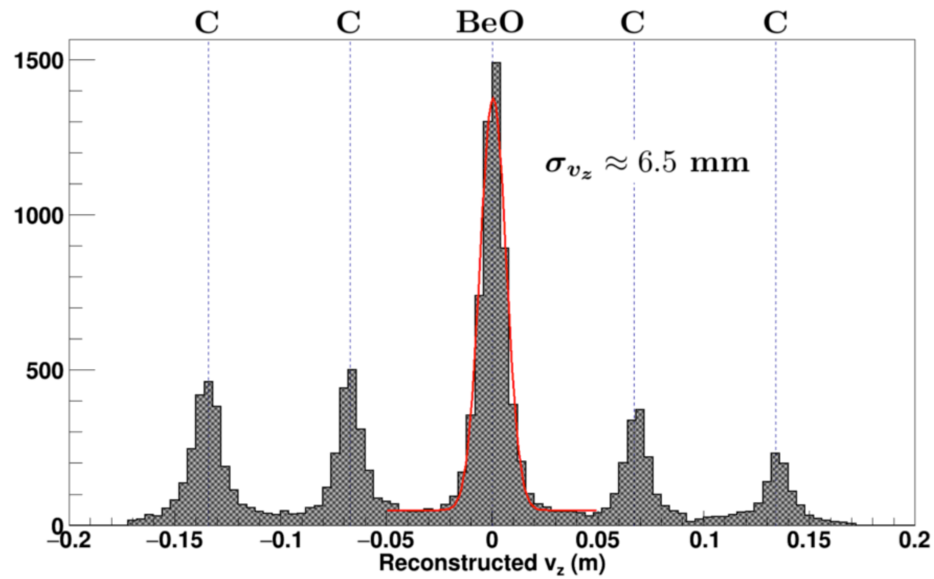

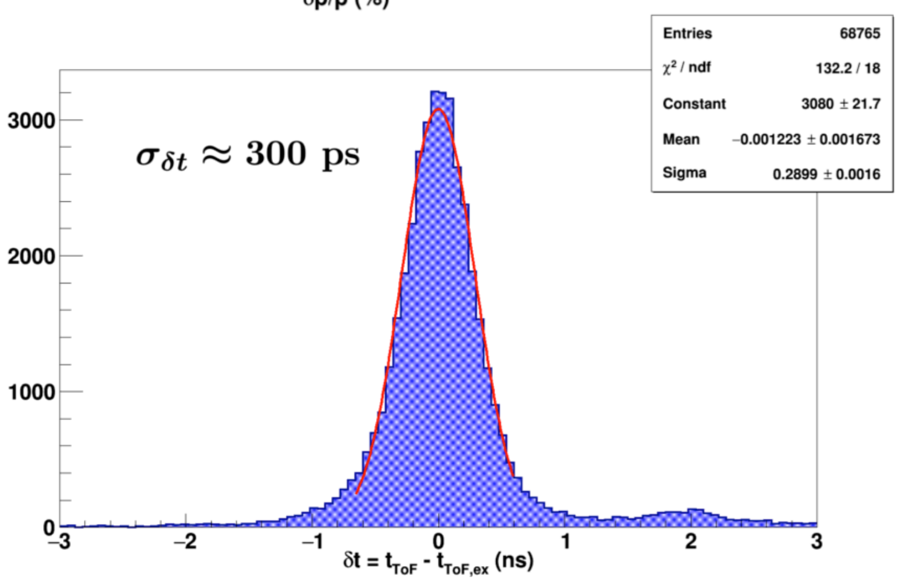

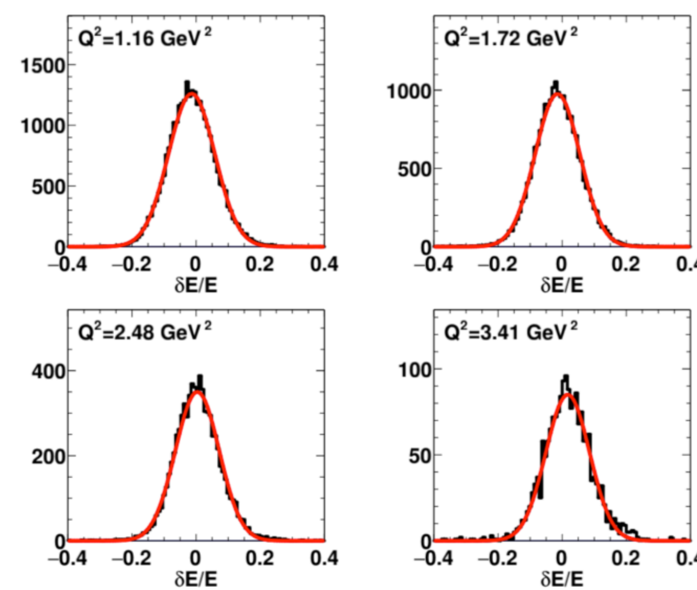

Neutron arm Kin. 1 Gain Calibration

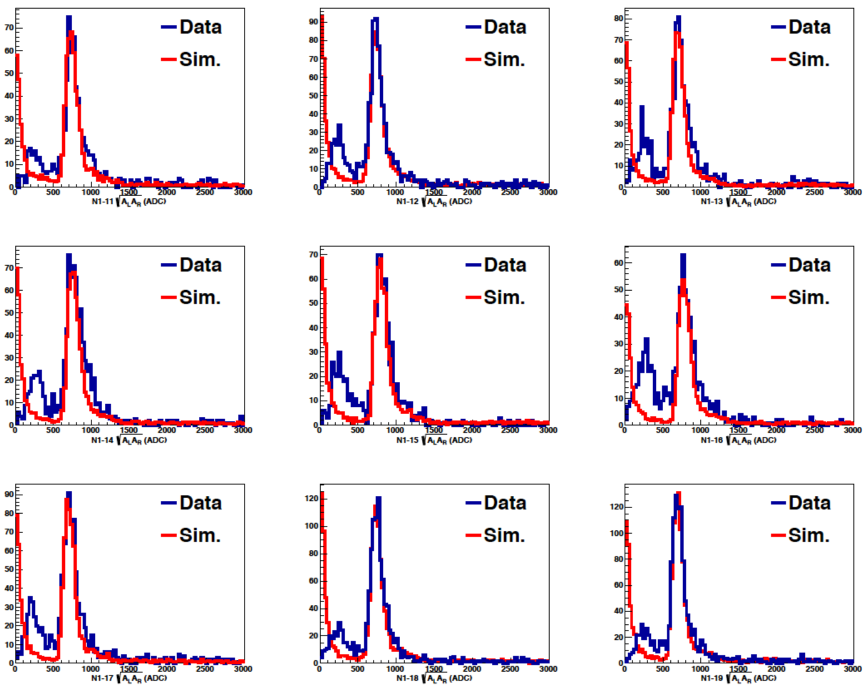

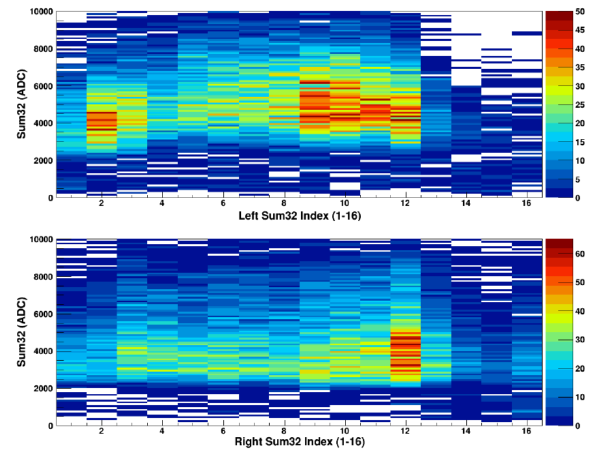

Fig. 5.45: The left and right maximum ADC sums of 32 blocks used to generate the T1 signal. The top (bottom) panel gets filled if the left (right) ADC sum32 is determined to be the maximum.

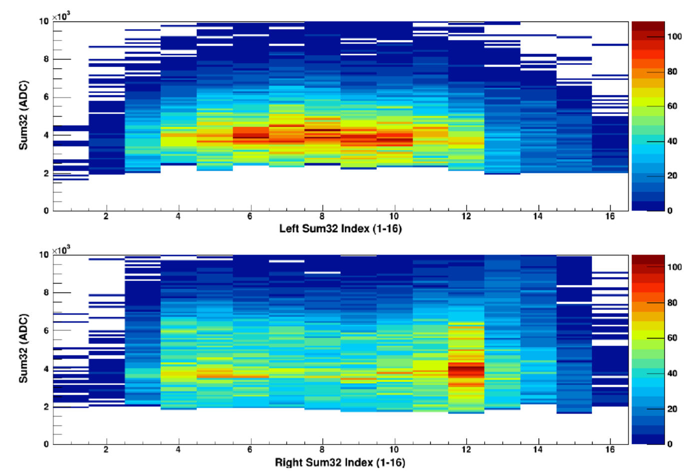

Fig. 5.48: Simulating the neutron detector left and right maximum sum32 signals where the thresholds are motivated by Figure 5.46.

- Neutron arm gain/trigger threshold calibration
- Detailed simulation of trigger logic including realistic channel-to-channel gain variations required to reproduce Kin. 1 nucleon misidentification probabilities/dilution factors

Quasi-elastic Event Selection: H_2 elastic data

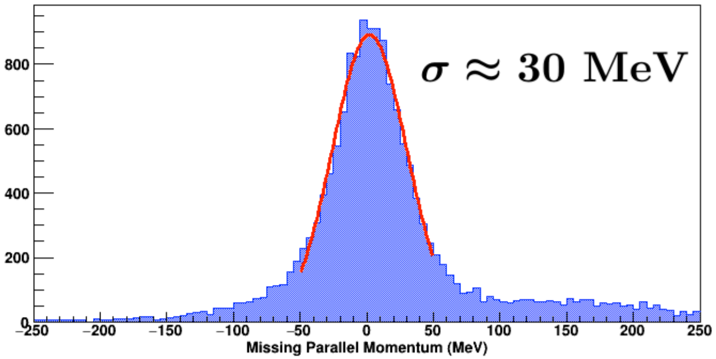

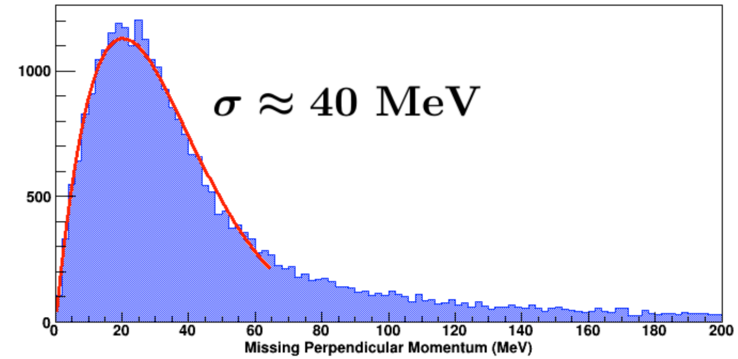

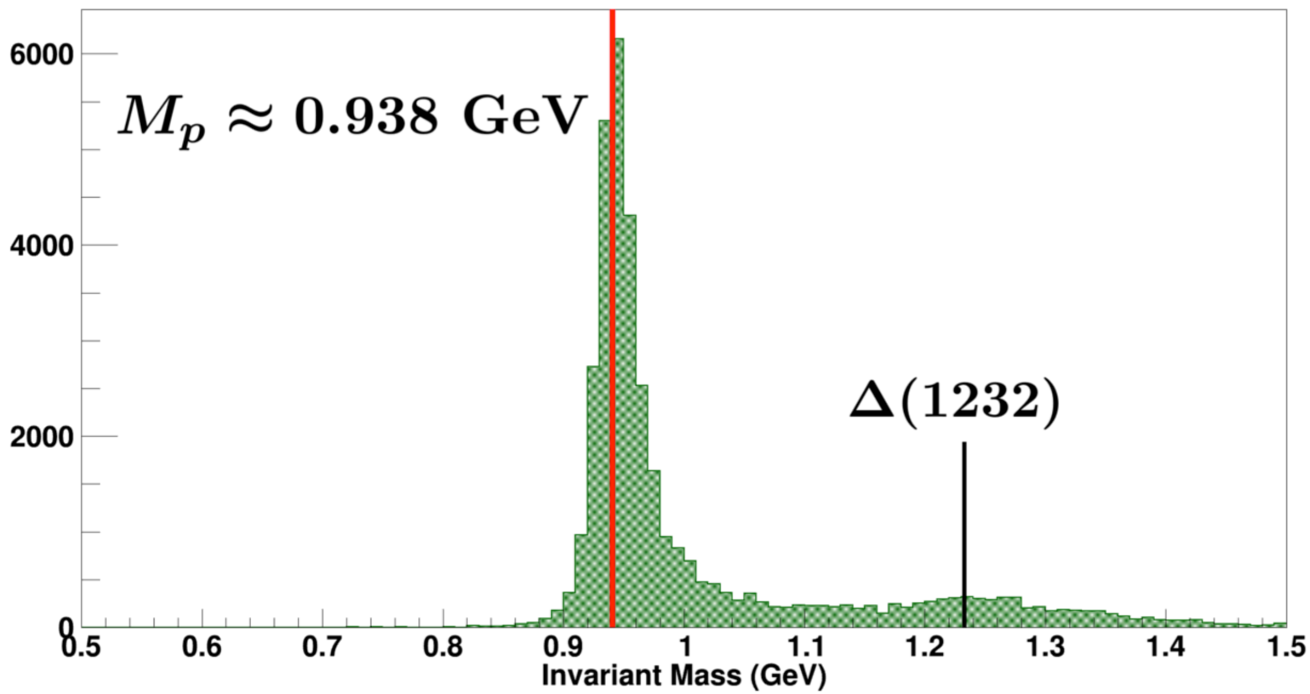

Inelastic Dilution: All kinematics

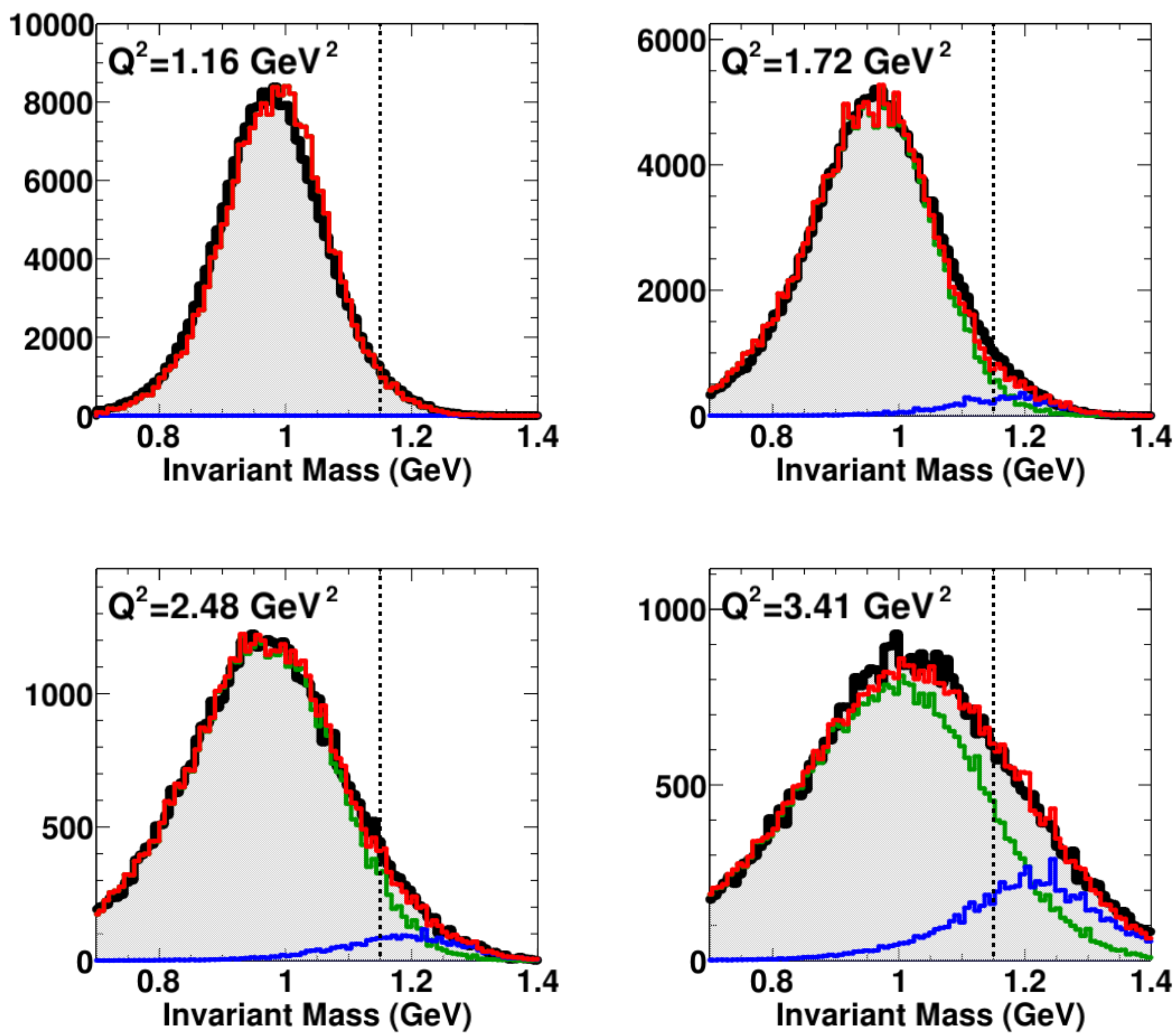

Random Background Dilution (Q^2=1.16 GeV^2)

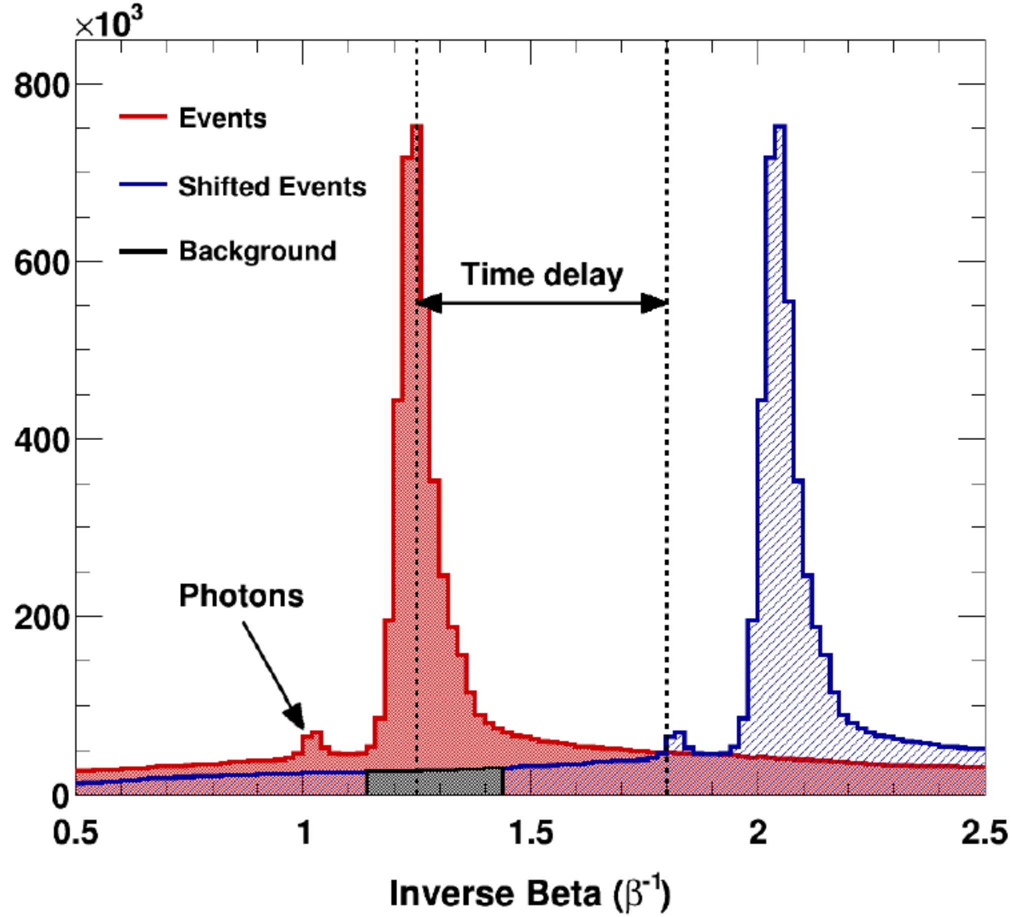

FIG. 20. (color online) The nucleon inverse β spectrum for the $Q^2 = 1.16$ GeV^2 data prior to applying the QE cuts (red), and displaying the procedure to estimate the background contribution (black) by artificially shifting the data in time (blue).

Pion dilution-–All kinematics

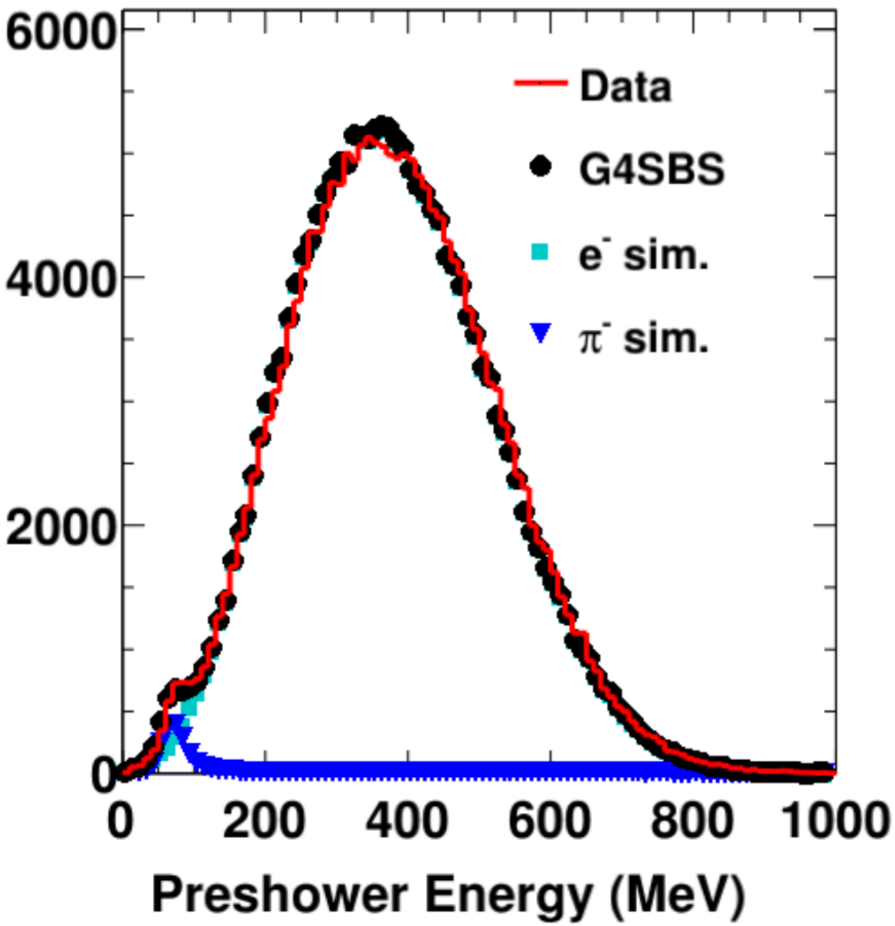

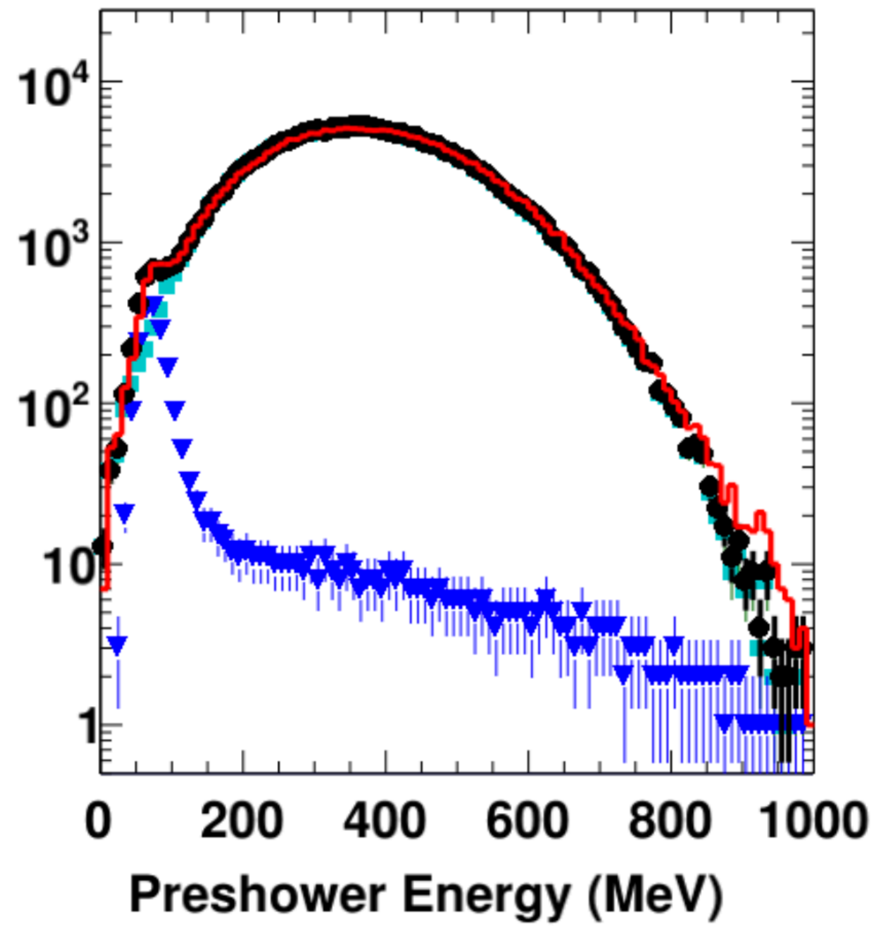

Proton Dilution ($Q^2 = 1.16$ GeV^2)

Parameter	Data	Simulation	Description
$\frac{\eta_p^n}{\eta_p^p}$	0.021 ± 0.002	0.020 ± 0.001	Protons observed as neutrons
$\frac{\eta_n^p}{\eta_p^p}$	Undetermined	0.384 ± 0.001	Neutrons observed as protons
$\frac{\eta_n^n}{\eta_p^p}$	0.559 ± 0.027	0.636 ± 0.001	Neutrons observed as neutrons
D_{p}	0.812 ± 0.017	0.839 ± 0.001	Proton dilution factor

Table: Charge ID results for the data and the simulation.

329

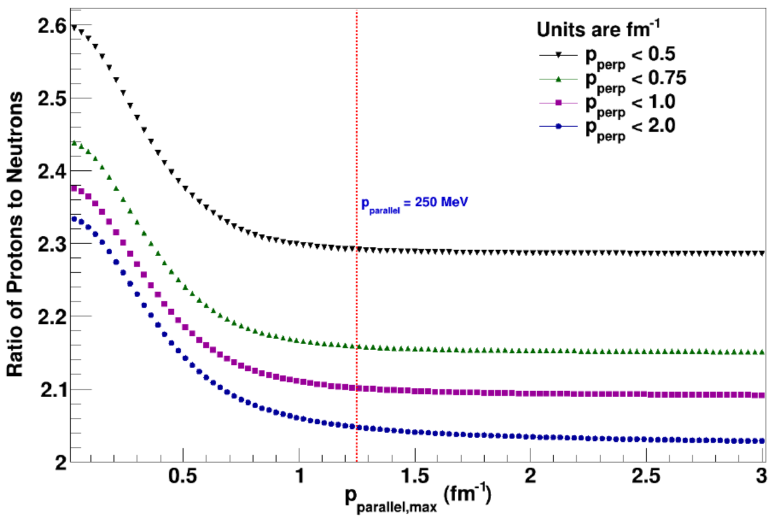

Fig. 5.69: The missing momentum dependence of the ratio of protons to neutrons for ^{3}He. Recall that 1 fm$^{-1} \approx 197$ MeV.

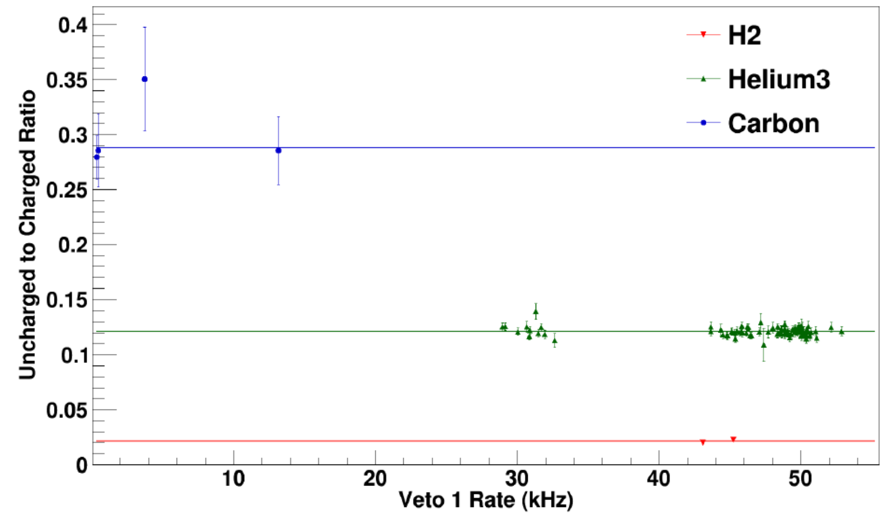

Fig. 6.4: The uncharged-to-charged ratio R and fit result for the three targets.

- The relevant nucleon misidentification probabilities are estimated from both the GEANT4 simulation and data using ”three-target” method and theoretical estimate of effective neutron/proton ratios passing quasi-two-body elastic kinematic cuts.

Nitrogen Dilution

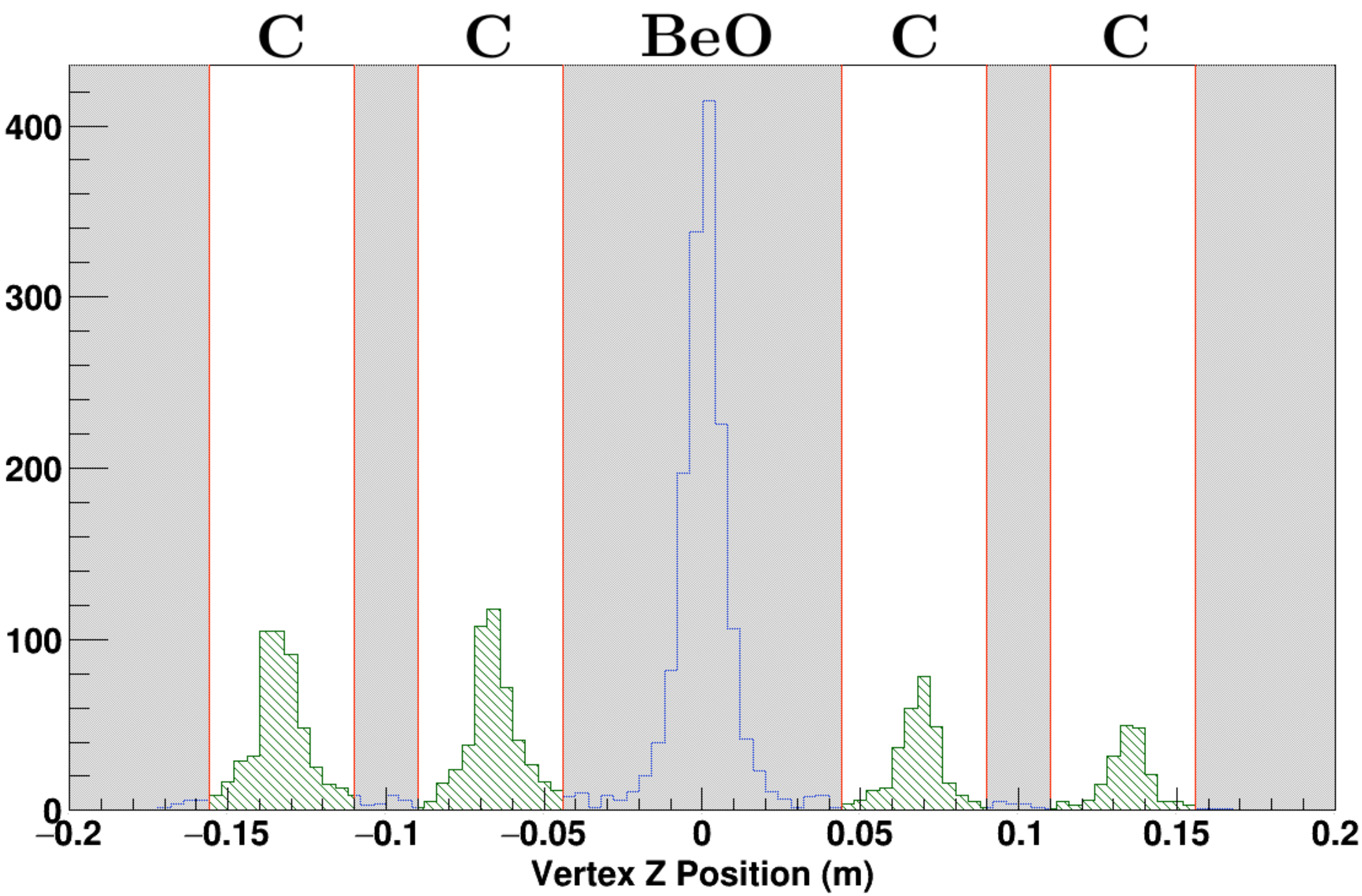

Carbon foil data used in lieu of N_2 ref. cell data for lowest Q^2